Emerging Era of Electrolyte Solvation Structure and Interfacial Model in Batteries

ACS Energy LETTERS

http://pubs.acs.org/journal/aelccp

FOCUS REVIEW

Emerging Era of Electrolyte Solvation Structure and Interfacial Model in Batteries

Haoran Cheng,[†] Qujiang Sun,[†] Leilei Li, Yeguo Zou, Yuqi Wang, Tao Cai, Fei Zhao, Gang Liu, Zheng Ma, Wandi Wahyudi, Qian Li,* and Jun Ming*

Cite This: *ACS Energy Lett.* 2022, 7, 490−513

Read Online

ACCESS | Metrics & More | Article Recommendations

ABSTRACT: Over the past two decades, the solid−electrolyte interphase (SEI) layer that forms on an electrode's surface has been believed to be pivotal for stabilizing the electrode's performance in lithium-ion batteries (LIBs). However, more and more researchers currently are realizing that the metal-ion solvation structure (e.g., Li^+) in electrolytes and the derived interfacial model (i.e., the desolvation process) can affect the electrode's performance significantly. Thus, herein we summarize recent research focused on how to discover the importance of an electrolyte's solvation structure, develop a quantitative model to describe the solvation structure, construct an interfacial model to understand the electrode's performance, and apply these theories to the design of electrolytes. We provide a timely review on the scientific relationship between the molecular interactions of metal ions, anions, and solvents in the interfacial model and the electrode's performance, of which the viewpoint differs from the SEI interpretations before. These discoveries may herald a new, post-SEI era due to their significance for guiding the design of LIBs and their performance improvement, as well as developing other metal-ion batteries and beyond.

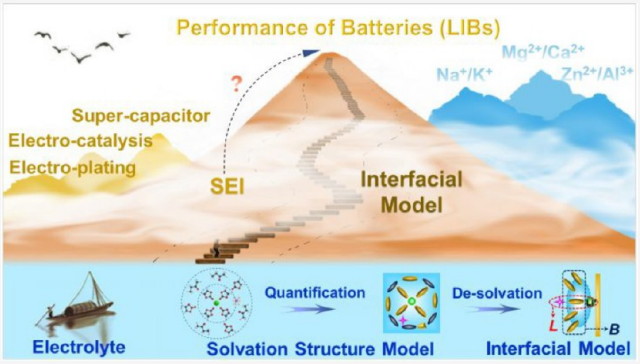

Lithium-ion batteries (LIBs) have come to dominate the field in energy conversion and storage area for portable electronic devices and electric vehicles (EVs), owing to their high energy density, beyond 300 Wh/kg.[1−4] It is commonly believed that the solid−electrolyte interphase (SEI), formed on an electrode's surface by electrolyte decomposition, can stabilize the electrode's performance in LIBs.[5−9] This viewpoint has contributed significantly to improving the performance of LIBs and has become a consensus over the past two decades,[10−15] which may be called the SEI era. Based on this understanding, engineering a robust SEI by regulating the electrolyte compositions (i.e., lithium salt, solvent, additives, etc.) has become a principle of electrolyte design (Figure 1a).[16−22] However, it remains a challenge to elucidate the relationship between the SEI and electrode performance since the SEI/electrode is more like a stiff "solid/solid" interface that lacks scientific correlations in liquid systems. This issue hinders efforts to design better electrolytes, as there is no clear guideline for figuring out which composition is beneficial or detrimental in the SEI, let alone forming the SEI that the electrode needs by controlling electrolyte decompositions.

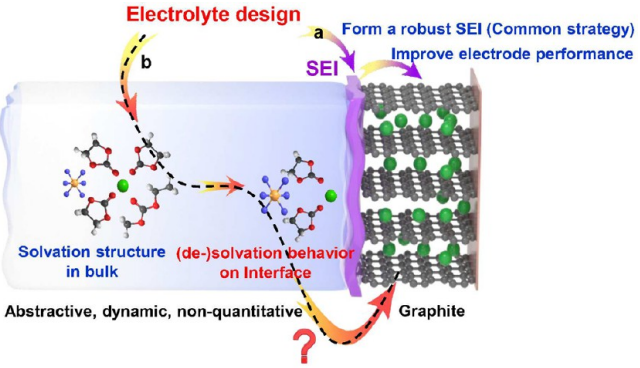

Figure 1. Electrolyte design principle for LIBs. (a) Empirical electrolyte design principle based on forming a good SEI. (b) Electrolyte design principle based on electrolyte solvation structure and Li^+ desolvation process. A typical graphite anode is used as an example.

Received: November 6, 2021
Accepted: December 22, 2021

https://doi.org/10.1021/acsenergylett.1c02425
ACS Energy Lett. 2022, 7, 490−513

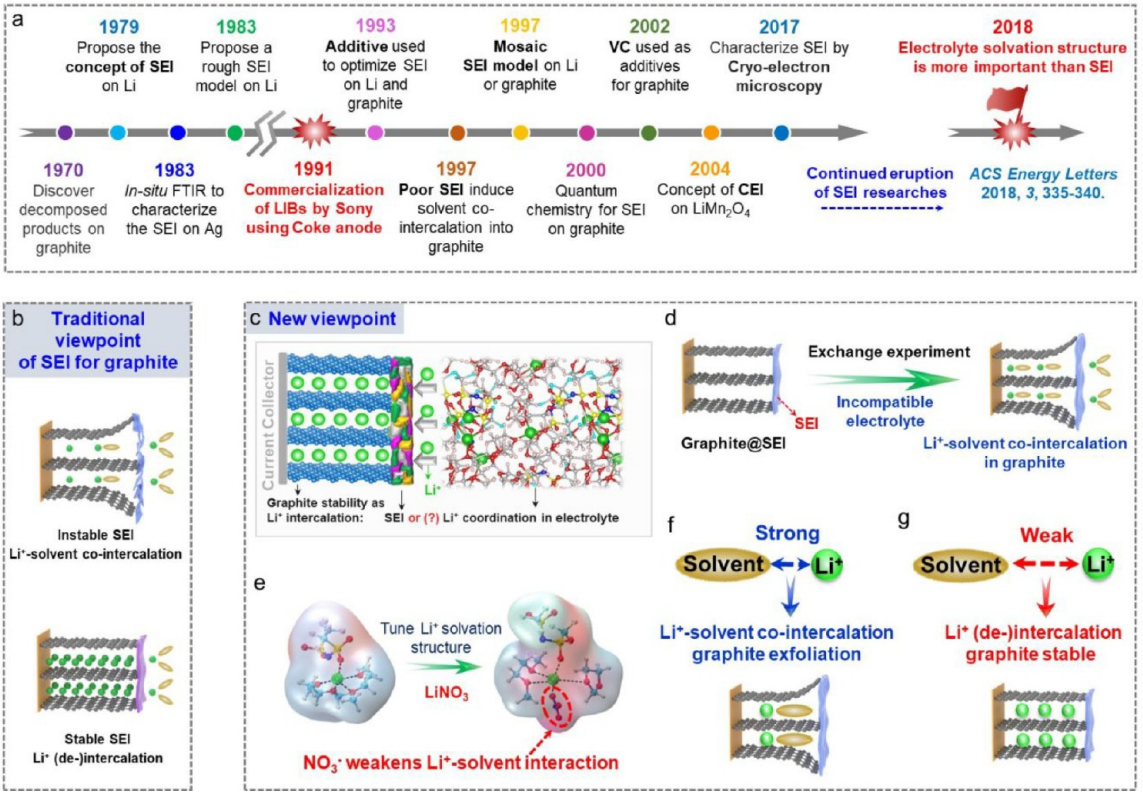

Figure 2. Importance of the solvation structure and controversy with regard to the SEI. (a) History of SEI development in batteries. (b) Traditional and (c) new viewpoints on the SEI effect on graphite performance. (d) Excluding the SEI effect by an exchange experiment using a graphite@SEI electrode in an incompatible electrolyte. (e) Snapshot of Li^+ solvation structure with and without $LiNO_3$ additives. (Reprinted with permission from ref 24. Copyright 2018 American Chemical Society.) (f, g) Correlation between Li^+ solvation structure (i.e., Li^+−solvent interaction) and graphite's performance.

From another point of view, changing the electrolyte composition can also change the lithium-ion solvation structure (i.e., Li^+) and thus influence the desolvation process on the electrode's surface. Besides the SEI effect, whether there is any scientific correlation between the changed Li^+ solvation structure, desolvation process, and the electrode performance is not fully understood. Recently, more and more researchers are realizing that the Li^+ solvation structure and desolvation process can affect an electrode's performance significantly.[23−37] However, it remains a challenge to illustrate the process, because the molecular behaviors in the bulk electrolyte and at the electrolyte−electrode interface are abstractive, dynamic, and non-quantitative.[38] Despite the findings on the effect of solvation structure in electrolytes, the battery performance has been ascribed to the solvation-structure-derived SEI that has a specific composition, thickness, and/or morphology,[39−42] which is an endless loop that fails to involve the specific solvation structure-derived interfacial model (i.e., Li^+ desolvation process) in the liquid since the battery performance is ascribed to the SEI again.[43−47] Thus, different viewpoints need to be clarified and emphasized to set direct scientific relationships between molecular interactions of electrolyte species and electrode performance, so as to make a breakthrough in this field and beyond.

Herein we present a timely review of recent research, focused on how researchers discover the importance of electrolyte solvation structure, develop a quantitative model to describe solvation structure, construct an interfacial model in LIBs to understand electrode performance, and then apply these discoveries in electrolyte design. This review focuses on the scientific relationships between the molecular interactions of electrolyte species (metal ions, anions, and solvents) in the interfacial model and the electrode performance. We unravel plenty of opportunities that enable us to design better electrolytes, while the classical SEI strategy is leading to a narrow opportunity. These discoveries are significant for designing LIBs and improving their performance in terms of life span, energy density, safety issues, and specific functions, which may herald a new era, that is, the post-SEI era, for LIBs, other metal-ion batteries (e.g., Na^+, K^+, Ca^{2+}, Ma^{2+}, Zn^{2+}, etc.), and beyond (e.g., supercapacitors, electrocatalysis, electroplating, etc.).

1. Discover the Importance of the Electrolyte Solvation Structure and Its Controversy with Respect to the SEI. Before presenting a different viewpoint, we first summarize the history of SEI development, the concept of which was proposed based on the electrolyte's decomposition products on the surface of a lithium metal anode in 1979, after the discovery of decomposion products on the surface of a graphite electrode (Figure 2a).[48,49] A rough SEI model that lacked a description of the decomposition products was proposed in 1983.[50] Later, the significant role of the SEI was fully demonstrated in an ethylene carbonate (EC)-based electrolyte, where a good SEI formed from the reduction of partial EC solvents, allowing a reversible Li^+ (de)intercalation within the carbon-based anode (e.g., graphite) and inhibiting the graphite exfoliation (Figure 2b), thereby enabling the commercialization of LIBs.[51] Besides, a good SEI can also

https://doi.org/10.1021/acsenergylett.1c02425
ACS Energy Lett. 2022, 7, 490−513

passivate the electrode surface and block electron transfer from the highest occupied molecular orbital/lowest unoccupied molecular orbital (HOMO/LUMO) of the electrolyte to the electrode.[52] In contrast, a poor SEI that forms in propylene carbonate (PC) or a normal ether-based electrolyte fails to support a reversible Li^+ (de)intercalation, leading to a severe Li^+−solvent co-intercalation and the exfoliation of the graphite electrode (Figure 2b).[53] The research on SEIs erupted fast due to the stabilization effect of the SEI on the electrode in LIBs. The concept of the functioning of the SEI and further studies on its properties rapidly followed the discovery of its positive effect on the graphite electrode. In addition, the discovery of film-forming additives (e.g., CO_2,[54] propylene sulfite (PS),[55] ethylene sulfite (ES)[56]) that can form a better SEI provided a new opportunity to study the SEI and further enhance the LIBs' performance. Since then, the classic mosaic model of SEI microstructure,[57] quantum chemical calculations for studying the SEI formation path and screening additives,[58,59] the model of the decomposition products on the surface of cathode (CEI),[60] and so forth have been presented and developed to understand the properties of the SEI. Among the reported studies, one of the greatest achievements is the discovery of vinylene carbonate (VC) as an additive,[61] which can enhance the graphite electrode's stability and boost the initial Coulombic efficiency. This discovery opens a new avenue to improve the LIBs' performance by choosing and designing effective additives to form a better SEI. Thus, the strategy of engineering the SEI has been utilized to guide the design of LIBs' electrolytes over the past two decades, based on which numerous film-forming additives have been reported,[62−69] and bunches of techniques (including cryo-electron microscopy)[70] have been developed to characterize and analyze the SEI, to further improve the LIBs' performance.[71−73]

The viewpoint on the stabilizing effect of the solid−electrolyte interphase on electrode performance was challenged in 2018.

However, the viewpoint on the stabilizing effect of the SEI on electrode performance was challenged in 2018.[24] Ming et al. found that the Li^+ solvation structure in the electrolyte dominates the performance of the graphite electrode (i.e., reversible Li^+ (de)intercalation or Li^+−solvent co-intercalation) (Figure 2c). This is because a graphite electrode precoated with an SEI layer (i.e., graphite@SEI) still failed to inhibit the destructive Li^+−solvent co-intercalation when an incompatible electrolyte (e.g., the normal ether-based electrolyte of 1.0 M LiTFSI in dioxolane/dimethoxyethane (DOL/DME)) was used in a designed exchange experiment (Figure 2d). The exchange experiment was designed and carried out as the follows: The graphite electrode was initially cycled several times in a compatible electrolyte (e.g., commercial EC-based electrolyte of 1.0 M $LiPF_6$ in EC/diethyl carbonate (DEC) (1/1 in v/v)) to form a good SEI. The SEI-coated graphite electrode was disassembled from the cell and then was reassembled in a new cell using an incompatible electrolyte after washing and drying the graphite@SEI electrode. Finally, a cycling test was conducted on the newly reassembled cell. As a result, severe Li^+−solvent co-intercalation and graphite exfoliation were observed when the graphite@SEI electrode was cycled in the incompatible ether-based electrolyte (Figure 2d). This discovery is unexpected, as a good SEI is commonly believed to effectively stabilize the graphite electrode and inhibit the Li^+−solvent co-intercalation into the electrode.

Furthermore, this study led to another groundbreaking discovery: that the ether-based electrolyte (e.g., 2.5 M LiTFSI in DOL/DME) became compatible with the graphite electrode after the introduction of 0.4 M $LiNO_3$, while previously only a high-concentration electrolyte (i.e., at least higher than 5.0 M) could make the ether-based electrolyte compatible with the graphite electrode.[74] According to the exchange experiment, the role of SEI was ruled out. The Li^+ solvation structure change was believed to account for the compatibility of the electrolytes with the graphite electrode, which demonstrated that a NO_3^- anion could enter the first solvation shell of the Li^+ solvation structure, weakening the Li^+−solvent interaction effectively (Figure 2e). Thus, a principle of how to design electrolytes compatible with the graphite electrode (i.e., inhibiting the Li^+−solvent co-intercalation) was presented, i.e., weakening the Li^+−solvent interactions by changing the electrolyte compositions. Briefly, a strong interaction leads to Li^+−solvent co-intercalation that generally destroys the structure of the graphite electrode and thereby causes the failure of the battery (Figure 2f), while a weak Li^+−solvent interaction benefits the reversible Li^+ (de)intercalation to ensure stable battery performance (Figure 2g). This viewpoint was further proved with the electrolyte for potassium-ion batteries, as will be summarized later.

Since this discovery, more and more researchers have realized the importance of the Li^+ solvation structure for the graphite electrode's performance.[75] For example, Zhang et al. reported that a unique solvation structure-derived LiF-rich SEI was formed on the surface of graphite in a DME-based localized high-concentration electrolyte (LHCE, 1.5 M LiFSI in DME/bis(2,2,2-trifluororthyl) ether (BTFE), 1/2 in v/v), making the electrolyte compatible with graphite for a reversible Li^+ (de)intercalation (Figure 3a).[76] In stark contrast, without dilution with BTFE, Li^+−solvent co-intercalation and graphite exfoliation were observed in the low-concentration electrolyte (LCE) due to the instability of the SEI (Figure 3b). The function of the solvation structure-derived SEI has been also demonstrated in recently designed electrolytes (e.g., 1.0 M LiFSI in 1,4-dioxane,[77] 0.9 M $LiPF_6$ in PC/DEC with 1 vol% fluoroethylene carbonate (FEC)[78]), making the electrolyte well compatible with the graphite electrode. With these interpretations for the compatibility, the focus moved to different Li^+ solvation structures, in turn forming different SEIs. Such interpretations differ from those related to the concentrated electrolyte reported before (e.g., glyme, DME, DOL),[79,80] sulfone (e.g., sulfolane (SL), tetramethylene sulfone (TMS), ethyl methyl sulfone (EMS)),[81−83] dimethyl sulfoxide (DMSO),[75,84] nitrile (e.g., acetonitrile, AN),[85,86] and phosphate (e.g., trimethyl phosphate, TMP)[87]-based electrolyte) and the LHCE (e.g., 1,1,2,2-tetrafluoroethyl-2,2,3,3-tetrafluoropropyl ether (TTE),[82,88] BTFE[89,90]-based electrolyte), where the compatibility was directly ascribed to the formation of a stable and/or anion-dominated SEI, without considering the role of the solvation structure.

The importance of the Li^+ solvation structure has also been demonstrated in lithium metal batteries, in which a specific SEI can be formed on the lithium metal anode to achieve high performance. For example, introducing NO_3^- into the Li^+ solvation structure promoted the decomposition of FSI^- in the ether-based electrolyte (e.g., DME) to form a uniform SEI rich

https://doi.org/10.1021/acsenergylett.1c02425
ACS Energy Lett. 2022, 7, 490−513

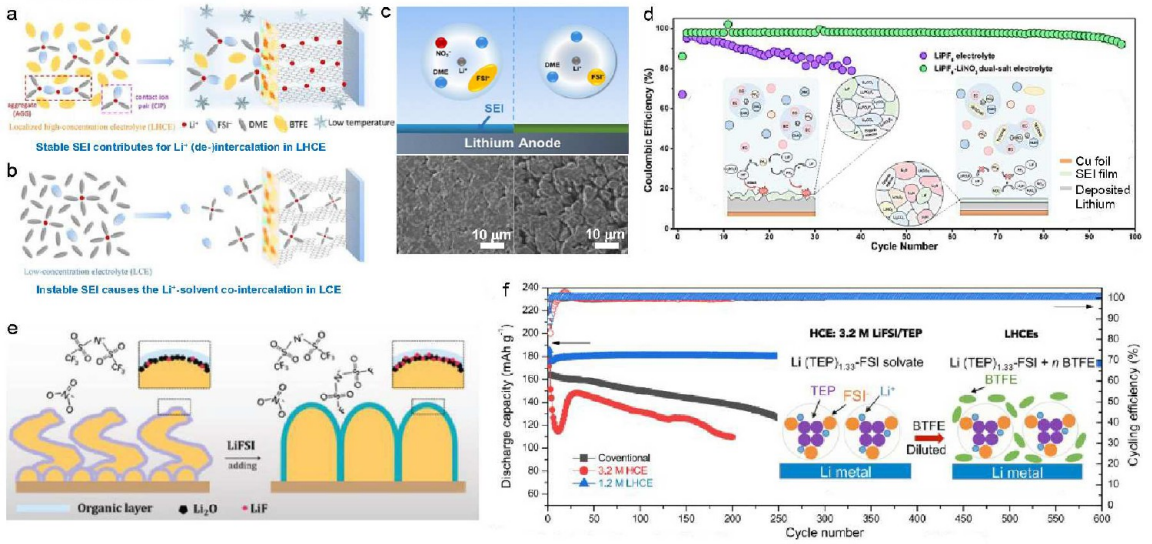

Figure 3. Solvation structure effect on electrode performance. Comparative illustration of Li^+ solvation structure and derived SEI effect on graphite's performance in DME-based electrolytes of (a) LHCE and (b) LCE with and without BTFE, and also for (c) the lithium deposition behaviors with and without $LiNO_3$. ((a, b) Reprinted with permission from ref 76. Copyright 2020 Wiley-VCH. (c) Reprinted with permission from ref 39. Copyright 2019 American Chemical Society.) Regulation of the solvation structure and the derived SEI by (d) adding $LiNO_3$ additive in the $LiPF_6$-based electrolyte, (e) increasing the LiFSI concentration in the DME-based electrolyte, or (f) introducing the BTFE diluent in the TEP-based electrolyte to improve the batteries' performances. ((d) Reprinted with permission from ref 91. Copyright 2021 American Chemical Society. (e) Reprinted with permission from ref 94. Copyright 2018 Wiley-VCH. (f) Reprinted with permission from ref 95. Copyright 2018 Elsevier.)

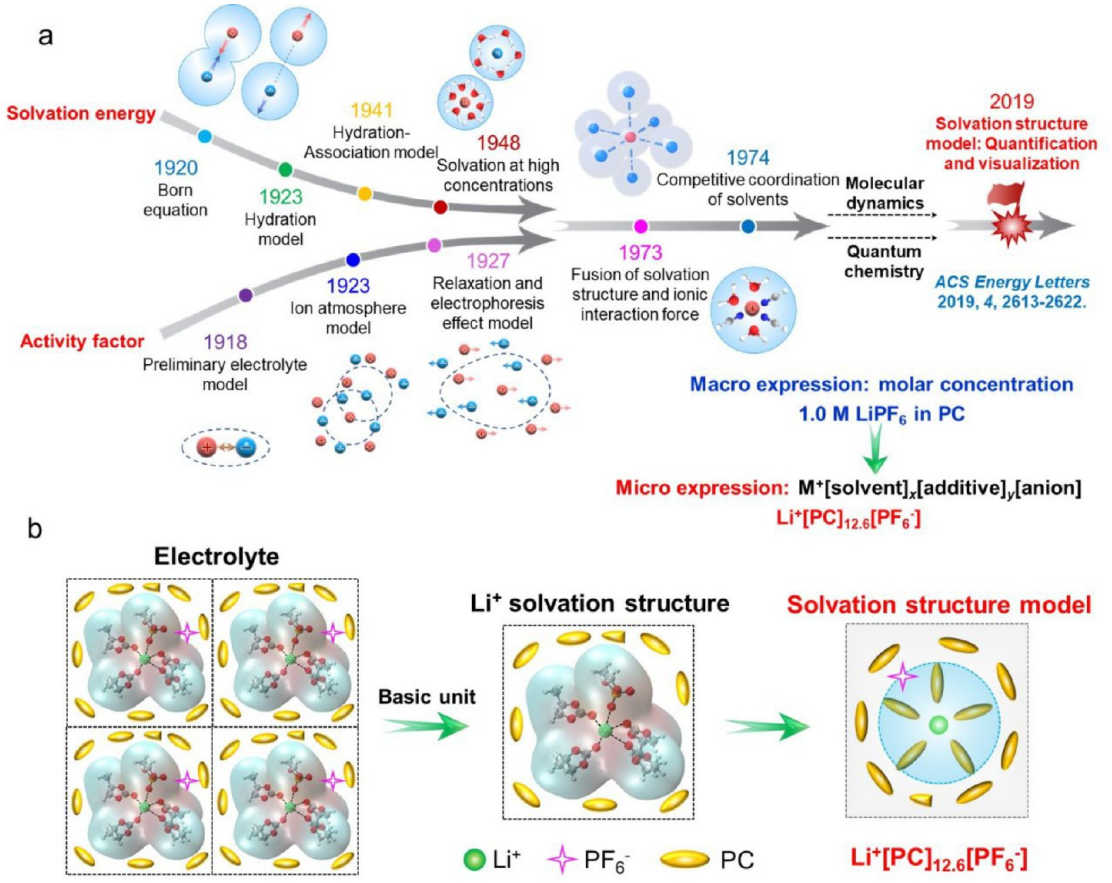

Figure 4. Methodology of how to describe the solvation structure. (a) History of the development of the solvation theory. (b) Proposed formula and model of the Li^+ solvation structure to describe the electrolyte quantitatively and graphically, instead of just with the molar concentration.

https://doi.org/10.1021/acsenergylett.1c02425
ACS Energy Lett. 2022, 7, 490−513

in $LiSO_x$, LiF, and LiN_xO_y, facilitating the development of safer lithium metal batteries without the formation of detrimental lithium dendrites (Figure 3c).[39] The positive effect of NO_3^- altering the Li^+ solvation structure (i.e., weakening the Li^+–PF_6^- interaction) to form a high ionic conductivity SEI was also observed in the triethylene glycol dimethyl ether (TEGDME)-based electrolyte, giving rise to a higher performance in the Li|Cu cell (Figure 3d).[91] Besides, regulating the Li^+ solvation structure by increasing the concentration of lithium salts (i.e., LiTFSI,[74] LiFSI[92−94]) also improved the formation of compact or Li_2O-LiF-rich SEI layers via the reduction of LiFSI and LiFSI/$LiNO_3$ to improve the stability of Li deposition (Figure 3e).[93,94] Moreover, tailoring the Li^+ solvation structure by adding BTFE into the electrolyte of 1.2 M LiFSI in flame-retardant triethyl phosphate (TEP) formed a robust FSI-derived LiF-rich SEI, which suppressed the lithium dendritic growth and unwanted side reactions, enabling a long-term cycling performance over 600 cycles for a Li|$LiNi_{0.6}Co_{0.2}Mn_{0.2}O_2$ (NMC622) battery (Figure 3f).[95] To this end, the solvation structure has been shown to play key roles in the batteries, so understanding its detailed microstructure is of utmost importance.

2. Develop a Quantitative Model to Study the Solvation Structure and Conduct Comparisons with Other Descriptions. Although the solvation structure has been discovered to be important in both LIBs and lithium metal batteries, its effect is still controversial. First, whether it is rational to attribute the high battery performance totally to the specific SEI formed by the solvation structure effect is questionable. If it is true, it means the interpretation moves from the solvation structure back to the SEI again, as reported previously. If not, we must decide how to investigate the solvation structure and clarify its relationship with the electrode's performance. This issue is extremely challenging as we look back at the history of how researchers have studied the (non-)aqueous solution structure. In particular, the development of the solvation structure model was sluggish since 1973, after the ion−solvent interaction was introduced into the Debye−Hückel theory that had only considered ion−ion interactions.[96−102] The "ionic solvation coordination" model reported in 1974 is the latest model,[103,104] which can be extended from water to non-aqueous electrolytes and also to binary solvent solutions with solvent competition coordination (Figure 4a).

> Although the solvation structure has been discovered to be important in both lithium-ion batteries and lithium metal batteries, its effect is still controversial.

In 2019, Ming et al. proposed a model with a simple formula for the Li^+ solvation structure to study the electrolyte (Figure 4b),[26] where the electrolyte was described in analogy to the crystalline material that has the "basic unit" (i.e., a unit cell), that is, the Li^+ solvation structure. The Li^+ solvation structure can be expressed microscopically with the formula $Li^+[solvent]_x[additive]_y[anion]$, in which the values of x and y were calculated based on the macroscopic molar concentration of the electrolyte. For example, the electrolyte of 1.0 M $LiPF_6$ in PC can be written as $Li^+[PC]_{12.6}[PF_6^-]$. In the Li^+ solvation structure, one Li^+ can coordinate with 4−6 PC units to form the first solvation shell, where the remaining 6−7 PC units reside in the second solvation layer, while the anion locates between the first and second solvation shells. Then, the electrolyte is composed of the infinite repetition of this Li^+ solvation structure. This representation is a quantitative description for electrolytes in which the ion−ion and ion−solvent interactions are both considered, facilitating the development of the electrolyte research more graphically.

The Li^+ solvation structure model can be used to substantiate the coordination role of additives (e.g., vinyl sulfate, DTD) graphically. Specifically, DTD can coordinate with the Li^+ and then weaken the Li^+−solvent interaction gradually in the first solvation shell, making the PC-based electrolytes compatible with graphite when the amount of DTD reached 6 wt% (i.e., $Li^+[DTD]_{0.73}[PC]_{12.6}[PF_6^-]$) (Figure 5a−c). Likewise, the same coordination effect of DTD has also been observed experimentally and described graphically by the Li^+ solvation structure model in the ether-based electrolyte of 1.0 M LiTFSI in DOL/DME (i.e., $Li^+[DTD]_{0.66}[DME]_{4.94}[DOL]_{7.36}[TFSI^-]$) and 1.0 M LiTFSI in TEGDME (i.e., $Li^+[DTD]_{0.66}[TEGDME]_{4.46}[TFSI^-]$) (Figure 5d,e). Briefly, these models reconfirm that the weakened Li^+−solvent interaction is the root cause for the compatibility between the graphite electrode and the electrolyte (i.e., reversible Li^+ (de)intercalation), similar to the effect of NO_3^-.[24] This viewpoint on the coordination role differs from the traditional viewpoint, in which the additives are commonly believed to form a good film on the electrode to improve the electrode's performance, such as forming a robust SEI on graphite by using a film-forming agent (e.g., DTD) to inhibit the Li^+−solvent co-intercalation. In this study, the SEI effect was excluded again according to an exchange experiment, in which the graphite@SEI could not inhibit the Li^+−solvent co-intercalation once the DTD additive was removed from the PC or ether-based electrolytes, demonstrating the importance of the Li^+ solvation structure. Thus, this model can clarify the effect of additives on Li^+ coordination that previously had never been reported before, supplementing the recognition of the additive's role in the electrolyte (Figure 5f).

The model of the Li^+ solvation structure was further demonstrated by using additives with different coordination capabilities. It was found that an additive with weak coordination capability (e.g., EC, VC) can also change the Li^+ solvation structure, but it is insufficient to make the PC and ether-based electrolyte compatible with graphite. This is because additives with weak coordination capability cannot weaken the Li^+−solvent interaction effectively, despite some of them (e.g., VC) having a good capability to form SEI.

To the best of our knowledge, that report was the first to describe electrolytes graphically and quantitatively based on the Li^+ solvation structure and the simplified formula of the Li^+ solvation structure. In most cases, besides the molecular simulations,[105−108] the Li^+ solvation structure is always presented in a simple schematic illustration (Figure 5g) and described using the Li^+/solvent ratio for the abstractive electrolyte, where the study is based on many spectroscopies and not yet using any quantitative model. For example, Xu et al. described the coordination of lithium ions with various ^{17}O nuclei in the Li^+-solvation sheath by monitoring the change in chemical shifts of ^{17}O nuclei in an EC/dimethyl carbonate (DMC) mixture with the entire range of EC/DMC ratios.[109] Watanabe et al. used pulsed gradient spin−echo (PGSE) NMR

https://doi.org/10.1021/acsenergylett.1c02425
ACS Energy Lett. 2022, 7, 490−513

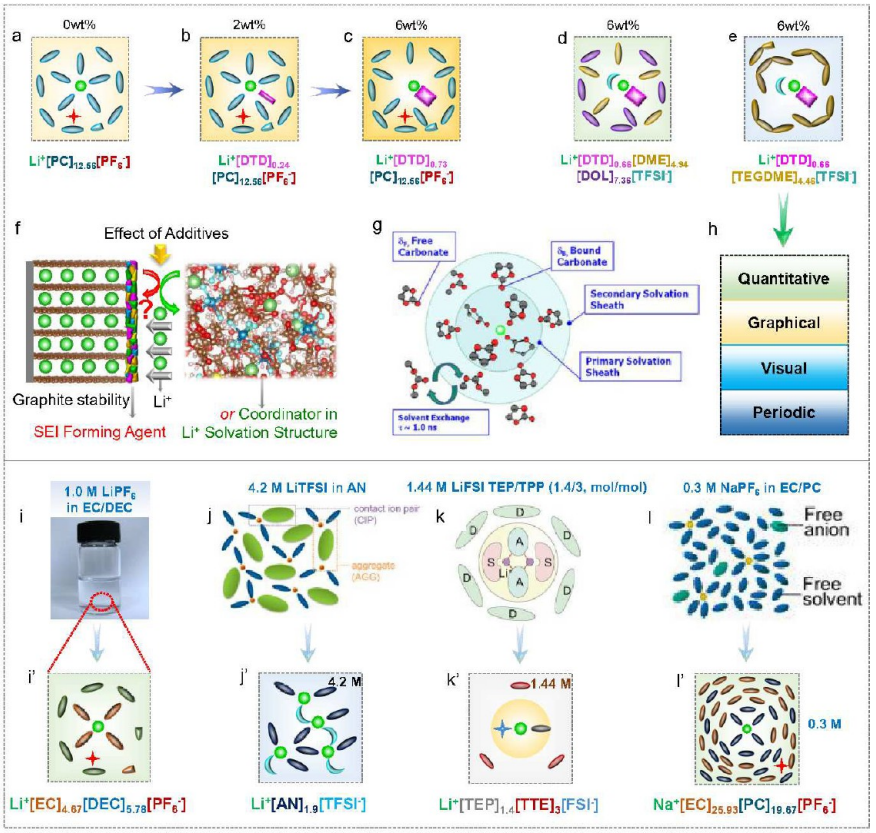

Figure 5. Description of Li^+ solvation structure and its applications. (a–c) Schematic of Li^+ solvation structures with different amounts of DTD additives in PC and ether, such as in (d) DOL/DME and (e) TEGDME-based electrolyte. (f) Discovery of the role of additive on graphite performance that can be described by the Li^+ solvation structure. (Reprinted with permission from ref 26. Copyright 2019 American Chemical Society.) (g) A typical description of the non-quantitative Li^+ solvation structure in electrolytes before. (Reprinted with permission from ref 109. Copyright 2013 American Chemical Society.) (h) Advantages of the presented Li^+ solvation structure model. Comparative description of the Li^+ solvation structure by (i–l) the traditional method and (i′–l′) the newly proposed method. (Reprinted with permission from ref 85. Copyright 2013 American Chemical Society. Reprinted with permission from ref 117. Copyright 2020 National Academy of Sciences. Reprinted with permission from ref 118. Copyright 2020 American Chemical Society.)

to measure the self-diffusion coefficient of solvents, lithium ions, and anions, where the formula $[Li(G3)_1][TFSA]$ (bis(trifluoromethanesulfonyl)amide (Li[TFSA]) in triglyme (G3)) was used to describe the electrolyte.[110] Likewise, the relationship between solvation number and temperature was also verified by Raman spectra.[111−114] Based on the ratio of solvent molecules to lithium ions, Abe et al. also proposed the formula of $Li(DMSO)_x(DMC)_y^+$ (e.g., 3.2 M LiTFSI/DMSO, 1.0 M LiTFSI/DMSO/DMC) to show a certain relationship between electrolyte compositions and graphite.[115] In addition, the average solvation numbers ($N_{PC,ave}$) of PC were also proposed using the concentration ratio (c_{free}/c_{solv}) of PC free of Li^+ and solvating Li^+ (e.g., N_{PC} = 3.7 in pure PC electrolyte). It was found that the PC/DMC-based electrolyte was compatible with graphite when the value of $N_{PC,\ ave}$ was less than 1.1.[116] However, research on how to quantitively describe the Li^+ solvation structure model in graphics and its effect on electrode performances has been rarely reported. According to the above discussion, the study Ming et al. presented can be evaluated as a landmark that built a relationship between the solvation structure and electrode performance by illustrating the Li^+ solvation structure in a quantitative, periodic, visible, and graphical way (Figure 5h), which is of great significance for the design of LIB electrolytes.

The Li^+ solvation model is applicable to describe the solvation structure of the electrolyte over a wide range of compositions, including the commercial electrolytes, the currently concentrated electrolytes, LHCE, and also the dilute ones. First, the commercial electrolyte of 1.0 M $LiPF_6$ in EC/DEC (1/1, v/v) can be described by the formula $Li^+[EC]_{4.12}$-$[DEC]_{7.73/88}[PF_6^-]$, in which the EC dominates the first solvation structure due to the higher binding energy of the Li^+−EC pair (Figure 5i,i′). In this way, about 10−13 solvent units stay around the Li^+ in a single Li^+ solvation structure in the 1.0 M electrolyte. Moreover, the formula of the Li^+ solvation structure has also been used to show the concentrated electrolyte, such as $Li^+[AN]_{1.9}[TFSI^-]$ for the electrolyte of 4.2 M LiTFSI in AN (Figure 5j,j′). It was found that only 1−3 solvent units surround the Li^+ in a single Li^+ solvation structure; thus, the concentrated electrolyte is more like an ionic liquid. Then, the anion can interact with the Li^+ and appears in the first solvation shell due to the insufficiency of solvents, weakening the Li^+−solvent interaction effectively. This is the reason why most concentrated electrolytes are compatible with the graphite electrode. Moreover, the Li^+ solvation structures in the typical LHCE (e.g., LiFSI/TTE, 1/3 in mol/mol in saturated TEP)[117] and dilute ones (e.g., 0.3 M $NaPF_6$ in EC/PC, 1/1 in v/v)[118] are represented by the formulas $Li^+[TEP]_{1.33}[TTE]_3[FSI^-]$ and $Na^+[EC]_{25.93}$-

https://doi.org/10.1021/acsenergylett.1c02425
ACS Energy Lett. 2022, 7, 490−513

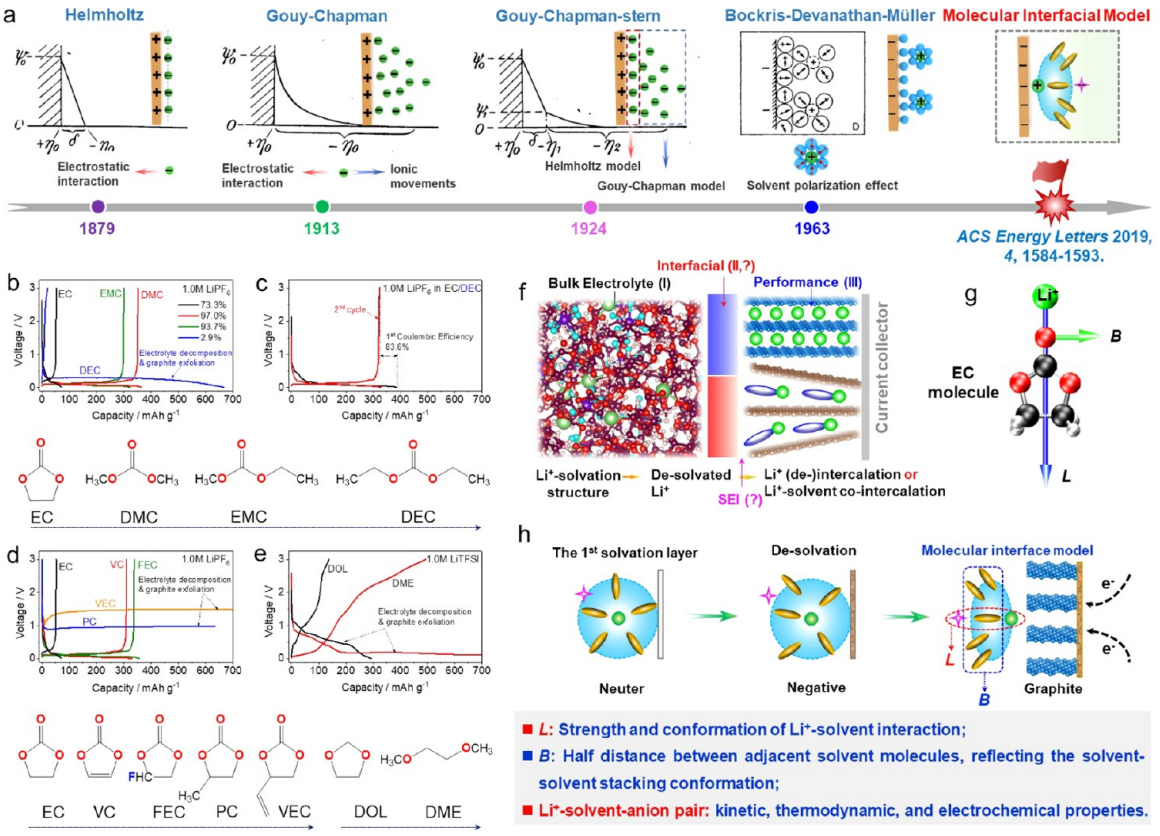

Figure 6. Solvation structure-derived molecular interfacial model. (a) History of the development of interfacial models (i.e., EDL). (Reprinted with permission from ref 125. Copyright 1924 Wiley-VCH. Reprinted with permission from ref 126. Copyright 1924 Elsevier.) (b–e) Unexplained different graphite performances in different electrolytes. (f) Correlation between bulk electrolyte, interfacial model, and graphite performance that needs to be explored. (g) Proposed *L* and *B* parameters using the EC molecule as an example. (h) Constructed molecular interfacial model on graphite electrode based on the Li^+ desolvation process. (Reprinted with permission from ref 25. Copyright 2019 American Chemical Society.)

$[PC]_{19.67}[PF_6^-]$, respectively, in which the interactions of metal ions, solvent, and anions could be described quantitatively and graphically (Figure 5k,k′, l,l′). According to the model, it is easy to deduce that the anion-derived SEI can be formed in the LHCE, because the anion can occupy the first solvation shell and be decomposed preferably.[117] In stark contrast, the anions in the dilute electrolyte that are far from the first solvation shell hardly participate in the decomposition, thereby inhibiting the HF generation.[118] While the purpose of both is to be able to form a stable SEI, the effect of the changed solvation structure has never been mentioned in the literature. Briefly, the comparison of the Li^+ solvation structure description presented in Figure 5i′–l′ shows that Ming et al.'s model provides a different view angle to analyze the electrolyte quantitatively and graphically.

3. Construct an Interfacial Model (i.e., Li^+ Desolvation Process) to Interpret Electrode Performance. Although the model of the solvation structure has been proposed, it is still hard to understand the electrolyte behaviors (i.e., Li^+ desolvation process) on the electrode's surface. This is the probable reason why Abe et al. reported that a certain relationship may exist between the solvation structure and the graphite compatibility,[116,119] but the relationship was not established until 2019.[25] This issue is related to the electric double layer (EDL) adjacent to the electrode surface during the electrochemical process (Figure 6a), a problem that has rarely been studied in LIBs and also is hard to study since the battery is a highly closed system. Moreover, the EDL is a dynamic and abstractive process which is hard to study on the molecular scale by any *operando* characterizations, let alone constructing a certain relationship with the electrode's performance. In stark contrast, the SEI has attracted greater attention, since it is concrete, visible, and easy to characterize.[120−122] However, we have to note that the SEI also is the product of electrolyte decomposition on the electrode, which means the electrolyte compositions (i.e., Li^+ solvation structure) and their behaviors on the electrode (i.e., Li^+ desolvation process) could be the main factors that affect the electrode performance.

> Although a model of the solvation structure has been proposed, it is still hard to understand the electrolyte behaviors on the electrode's surface.

The EDL in electrochemical systems experienced the development of several classic models, including those of Helmholtz (i.e., compact layer with electrostatic interaction),[123] Gouy−Chapman (i.e., dispersive layer with electrostatic interaction and ionic movements),[124] and Gouy−Chapman−Stern (i.e., a combination of Helmholtz and Gouy−Chapman models)[125] from 1879 to 1924. In 1963, the Bockris−Devanathan−Müller model was further developed

https://doi.org/10.1021/acsenergylett.1c02425
ACS Energy Lett. 2022, 7, 490−513

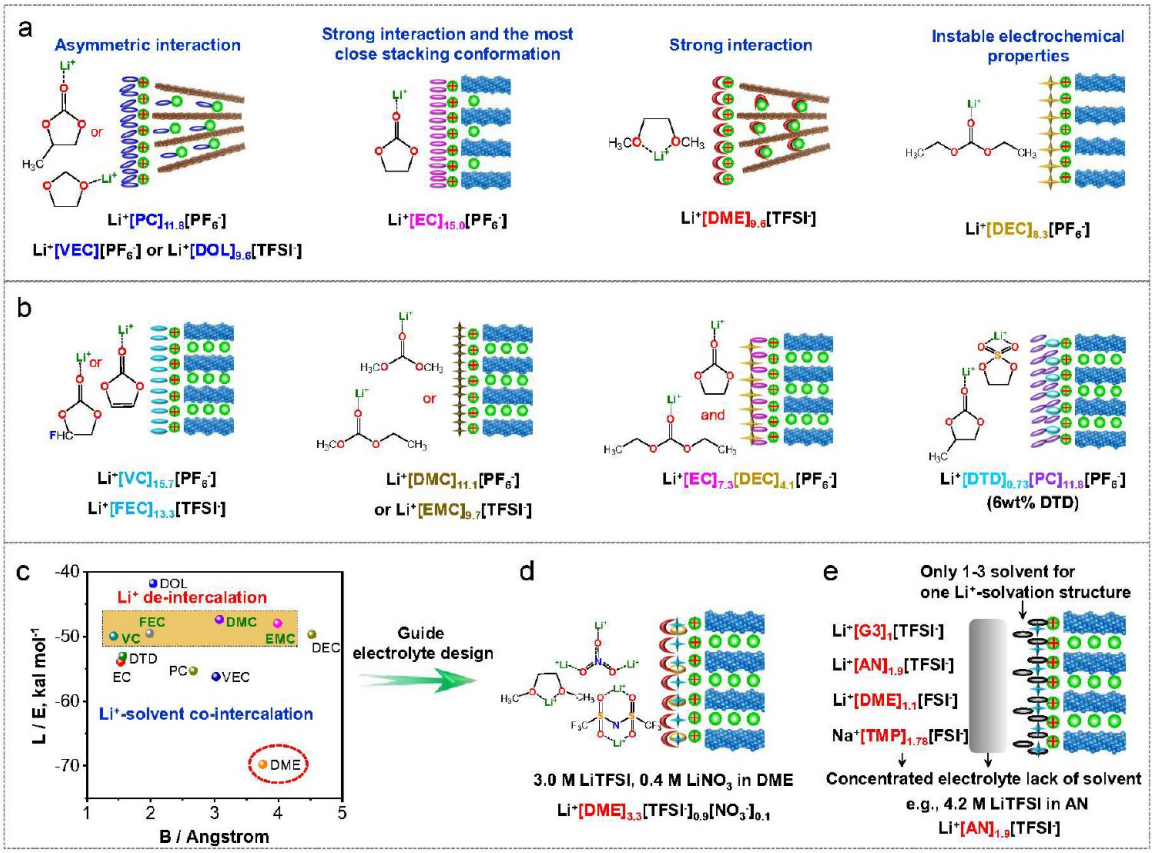

Figure 7. Correlation between interfacial model and graphite performance. (a) Cases of Li^+−solvent calation or electrolyte decomposition. (b) Cases of Li^+ reversible (de)intercalation due to the moderate Li^+−solvent interaction (*L*) and solvent−solvent stacking conformation (*B*). (c) Coordinate system showing the compatible (i.e., yellow area) and incompatible areas (blank area) for the electrolyte, based on (d) tuning the interfacial model to make the DME-based system compatible with graphite. (e) Interfacial model showing how the concentrated electrolyte is compatible with the graphite. (Reprinted with permission from ref 25. Copyright 2019 American Chemical Society.)

by considering the dipolar polarization of interfacial solvents, yet the effect of the H-bond interaction was still out of consideration.[126] Afterward, Gongadze et al. used the cavity field method to consider the mutual influence of water molecules and the orientation sequence of the water dipole in the concentrated electrolyte.[127,128]

However, studies on the EDL in LIBs were rarely reported, until the new interfacial model derived from the Li^+ solvation structure was proposed by Ming et al. in 2019.[25] This innovation was inspired by the observed different performance of graphite (i.e., Li^+−solvent co-intercalation or Li^+ (de)intercalation) in electrolytes when the single carbonate or ether solvent-based electrolytes were used.[25] For example, 12 different (dis-)charge curves can be observed in 12 different electrolytes in Figure 6b−e.

Based on these different graphite performances, some important questions have been raised: (i) how to interpret the low capacity and high polarization in EC electrolyte; (ii) how to interpret that both DMC electrolyte and ethyl methyl carbonate (EMC) electrolyte are compatible with a graphite electrode while the DEC electrolyte is incompatible; (iii) how to understand that the EC/DEC-based electrolyte becomes compatible with the graphite while the EC and DEC electrolyte are incompatible when used as a single solvent separately; (iv) how to interpret that different substitution of a H atom in the cyclic carbonate structure could give rise to different graphite performance, such as for those cyclic carbonate solvents of EC, FEC, PC, and vinyl ethylene carbonate (VEC) that have similar structures; (v) how to explain why most ether-based electrolytes (e.g., DOL, DME) are incompatible with graphite, and so forth. Understanding all of these phenomena is hard from the SEI viewpoint, stimulating researchers to consider other probable interpretations beyond the SEI concept. It is still questionable whether there is a general model that can explain these performance differences and also predict the performance—that is, which interfacial model can cause the Li^+−solvent co-intercalation and which interfacial model is good for the reversible Li^+ (de)intercalation (Figure 6f).

With the thoughts above, Ming et al. constructed a new interfacial model to address these issues, of which *L* and *B* parameters were proposed based on the Li^+ desolvation process (Figure 6g). *L* means the interaction strength and conformation of the Li^+−solvent, while *B* means half the distance between adjacent solvent molecules, reflecting the solvent−solvent stacking conformation surrounding Li^+ during the Li^+ desolvation process. A lower *B* value means easier formation of the closest packing on the surface of the electrode, such as the EC molecules. Additionally, the kinetics, thermodynamic properties, and electrochemical stability of the Li^+−solvent−anion complex were also proposed on the surface of the electrode to study the electrolyte behaviors, including how to evaluate and predict the electrolyte's stability (Figure 6h).

https://doi.org/10.1021/acsenergylett.1c02425
ACS Energy Lett. 2022, 7, 490−513

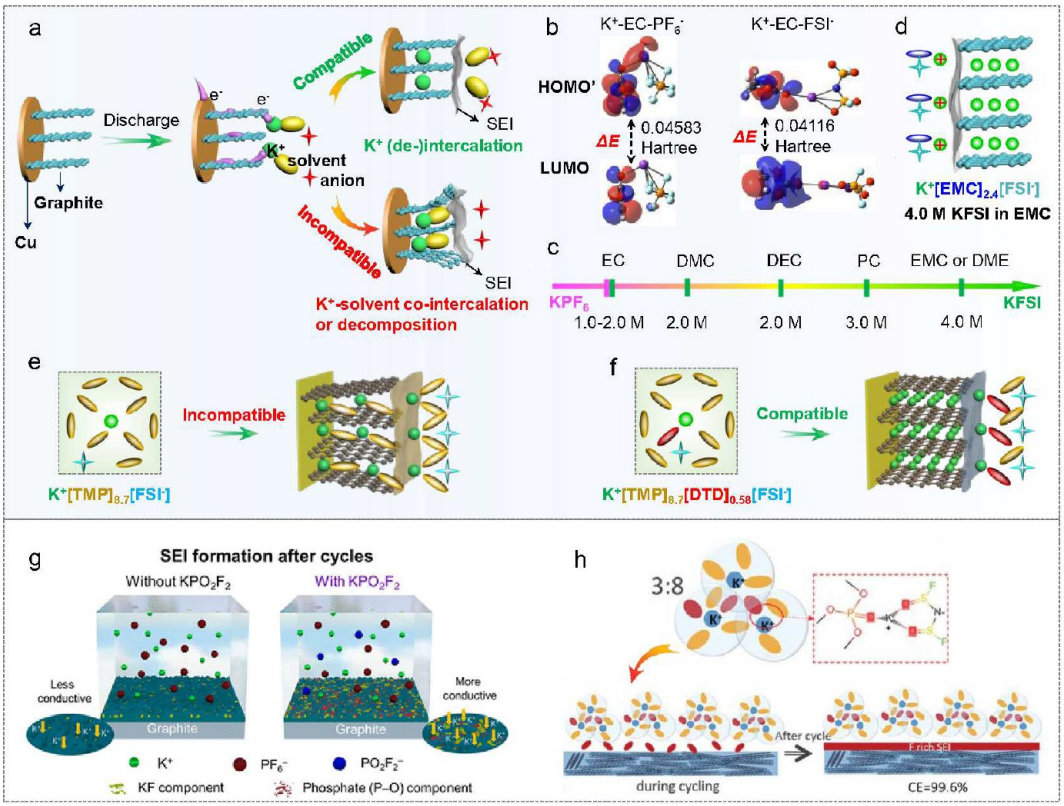

Figure 8. Design graphite-anode-compatible electrolytes in KIBs. (a) Competitive reaction pathways for K^+−solvent structure. (b) Comparison of the HOMO′ and LUMO levels of K^+-EC-PF_6^- and K^+-EC-FSI^-. (c) Compatible electrolyte concentrations using different potassium salts and solvents. (d) Interfacial model of 4.0 M KFSI in EMC compatible with graphite. (Reprinted with permission from ref 29. Copyright 2020 American Chemical Society.) Varied K^+ solvation structure, interfacial model, and graphite performance in the electrolyte of 1.0 M KFSI in TMP without (e) and with (f) DTD additives. (Reprinted with permission from ref 28. Copyright 2020 Wiley-VCH.) (g) Comparison of SEIs formed on graphite without KDFP (left) and with KDFP (right). (Reprinted with permission from ref 136. Copyright 2020 American Chemical Society.) (h) Solvation structure and the derived SEI formed on graphite in the electrolyte of KFSI/TMP (3/8 in mol/mol). (Reprinted with permission from ref 135. Copyright 2020 Wiley-VCH.)

Next, a series of molecular interfacial models were constructed based on the interaction and conformation of Li^+−solvent (L) and solvent−solvent (B), explaining why different graphite performances were observed in different electrolytes. When the interaction and/or conformation (i.e., L) of Li^+−solvent is asymmetric (e.g., Li^+-PC, Li^+-VEC, Li^+-DOL), strong and crowded (e.g., Li^+-EC, the lowest value of B for EC), or thermodynamically unstable (e.g., Li^+-DEC), Li^+−solvent co-intercalation or electrolyte decomposition occurs (Figure 7a). In contrast, a reversible Li^+ (de)intercalation can be achieved when the of Li^+−solvent and solvent−solvent (e.g., Li^+-VC, Li^+-FEC, Li^+-DMC, Li^+-EMC) interactions and/or conformations (i.e., L, B) are moderate. Besides, the values of L and B could be tuned readily by mixing the solvents (e.g., Li^+-EC/DEC) or adding additives (e.g., Li^+-DTD/PC), resulting in good compatibility of the electrolytes with graphite electrodes (Figure 7b). For example, a zigzag interfacial model could be formed on the surface of the graphite electrode in the EC/DEC-based electrolyte. It was found that the EC could arrange closer to the graphite surface due to the stronger Li^+-EC interaction and lower B value (i.e., molecular structure in small size with high freedom), while the DEC could arrange behind the EC to reduce the Li^+-EC interaction. Then, Li^+ could be desolvated readily and the decomposition of DEC could be avoided, allowing a reversible Li^+ (de)intercalation (Figure 7b). Likewise, the Li^+-PC interaction on the graphite surface could be also weakened by adding DTD additives into the electrolyte to achieve a reversible Li^+ desolvation (Figure 7b). Briefly, this model explains the different performances in completely different electrolytes, particularly showing how the Li^+−solvent interaction and additive affect the graphite performance from the aspect of an interfacial model rather than the SEI.

In addition, the L and B values and the graphite performances in the different electrolytes using a single solvent were further summarized, and they are divided into compatible (i.e., the yellow area) and incompatible areas (the blank area) in the coordinate system (Figure 7c). In this way, researchers could change the kind of solvent, anion, additive, and salt concentration to tune the L and B values in the interfacial model toward the yellow area, making the incompatible electrolyte in any blank area compatible, guiding the electrolyte design. For example, increasing the lithium salt concentration (i.e., LiTFSI) to 3.0 M and adding 0.4 M $LiNO_3$ additive into DME-based electrolytes can make such an extremely incompatible electrolyte compatible with graphite, which enables a reversible Li^+ (de)intercalation (Figure 7d). According to the interfacial model, it is also easy to understand why the concentrated electrolyte (e.g., AN,[85] DME,[79] G3,[129] TMP-based[130] electrolyte) is compatible with graphite. This is because the solvent is insufficient (i.e., only 1−3 solvent units around the Li^+) and has to stay in the electrolyte to dissolve

https://doi.org/10.1021/acsenergylett.1c02425
ACS Energy Lett. 2022, 7, 490−513

the lithium salt; otherwise, the lithium salt could precipitate from the electrolyte if the solvent is co-intercalated with the Li^+ into graphite (Figure 7e).

Herein, researchers may consider the SEI effect on the graphite performance as before, regardless of the interfacial model. The preliminary results of Ming et al.'s studies indicate that the SEI can reduce the direct contact between the electrode and electrolyte and then mitigate the electrode's electron-donating capability to the Li^+−solvent−anion complex, which in turn increases the electrolyte's stability (e.g., electrochemical stability of Li^+−solvent−anion). Overall, different from the SEI, the molecular interfacial model presented in this section successfully explains and predicts graphite's performance, which can be further applied to interpret the different lithium deposition phenomena in the different electrolytes. This is a breakthrough that deserves to be emphasized since it may change our thoughts in designing the electrolyte and understanding the electrode's performance. This model has great potential to be applied to a broad electrochemical system that involves the electrolyte−electrode interface, which includes but is not limited to electrode-plating, supercapacitors, and electrocatalysis.

Notably, while this molecular interfacial model is similar to the EDL in electrochemistry, the relationship between the molecular interfacial model and the electrode's performance is more direct and graphical. More recently, the interfacial molecular behaviors in batteries have attracted great attention since they can influence an electrode's performance significantly. For example, Zhang et al. proposed that an inner Helmholtz layer was generated at the electrode interface before the formation of the SEI.[38] This EDL is composed of solvent and competitively adsorbed anions, which play an important role in the formation of the initial SEI. Pan et al. also demonstrated that the distances and activation energies that lithium ions transport across the inner Helmholtz layers affect the polarization in batteries.[131] Briefly, the studies discussed in this section provide a new angle to understand a battery's performance based on the molecular interfacial model.

4. Apply the Solvation Structure and Interfacial Model in Metal-Ion Batteries. *4.1. Design Graphite-Anode-Compatible Electrolytes in Potassium-Ion Batteries.* The proposed solvation structure and interfacial model were applied in potassium-ion batteries (KIBs) to address the major issue of electrolytes that were incompatible with graphite electrodes, achieving a reversible K^+ (de)intercalation.[132,133] Ming et al. proposed two competitive interfacial reaction pathways for the M^+−solvent−anion complex (e.g., $M^+ = K^+$) during the K^+ desolvation process.[29] In the first pathway, the K^+−solvent−anion complex can be desolvated when it accepts one electron from the electrode, releasing the free K^+ that can be (de)intercalated into the graphite. This pathway is preferred and can make the electrolyte compatible with graphite. Alternatively, the K^+−solvent−anion complex can be decomposed if the K^+−solvent interaction (i.e., L) is strong or the thermodynamic or electrochemical stability of the K^+−solvent−anion complex is insufficient, leading to the K^+−solvent co-intercalation (i.e., graphite exfoliation) and/or electrolyte decomposition. The latter pathway occurs when the electrolyte is incompatible with the graphite electrode (Figure 8a).

The parameter ΔE (i.e., the energy difference between two pairs of orbitals, the highest occupied molecular orbital′ (HOMO′)−lowest unoccupied molecular orbital (LUMO)) was also proposed to evaluate the stability of the K^+−solvent−anion complex, where a higher ΔE means a more stable electrolyte due to the big difference in orbitals and the difficulty to transfer the electron (Figure 8b). The LUMO is used to designate the critical orbitals for the K^+−solvent−anion complex, where the corresponding orbitals become HOMO′ after obtaining one extra electron from the electrode. For example, the stability of K^+-EC-PF_6^- is higher than that of K^+-EC-FSI^- after accepting one electron due to the higher ΔE (i.e., 0.04583 vs 0.04116 hartree). This result is consistent with the improved stability and compatibility of 1.0 M KPF_6 in EC compared to that of 1.0 M KFSI in EC.

Increasing the potassium salt (e.g., KFSI) concentration or changing the kind of solvent can alter the K^+−solvent−anion interaction (i.e., L) and solvent stacking forming (i.e., B) in the interfacial model, which makes it possible to design better electrolytes that are compatible with graphite (Figure 8c). For example, the newly designed 4.0 M KFSI in EMC (i.e., $K^+[EMC]_{2.4}[FSI^-]$) is compatible with the graphite electrode due to the reduced K^+−solvent interaction and sufficient stability of the K^+−solvent−anion in the interfacial model (Figure 8d). According to this principle, using an additive with strong coordination capability (e.g., DTD) results in a good compatibility of TMP-based electrolyte with graphite.[28] This is because the DTD can regulate the K^+ solvation structure from $K^+[TMP]_{8.7}[FSI^-]$ to $K^+[TMP]_{8.7}[DTD]_{0.58}[FSI^-]$ and then alter the interfacial model (i.e., reduce the K^+-TMP interaction) so that the K^+ could be effectively desolvated at the electrolyte−graphite interface and then reversibly (de)intercalated into the graphite (Figure 8e,f).[134,135]

The strategy of tuning the interfacial model differs from those of forming an SEI by employing additives (e.g., potassium difluorophosphate, KDFP) and/or pretreatment in specific conditions (e.g., precycled in the electrolyte of 1.0 M KPF_6 in EC/DME at 50 °C) to make the electrolyte compatible with the graphite.[136,137] For example, a KF and PO_x species-rich SEI can be formed on graphite electrodes by using KDFP additives, which improves the K^+ (de)intercalation kinetics, capacity retention, and Coulombic efficiency (Figure 8g).[136] This research is similar to those developed in LIBs, such as in the PC-based electrolyte.[138−142] Although more and more researchers have realized that the K^+ solvation structure plays a decisive role in graphite's performance, the interpretations are always ascribed to the formation of a robust and stable solvation-structure-derived SEI. For example, a stable KF-rich SEI layer was formed on the graphite surface due to the formation of a unique solvation structure in an LHCE (i.e., concentrated KFSI/DME electrolytes with 6.91 mol kg^{-1} KFSI in DME) after the addition of a highly fluorinated ether (HFE), inhibiting the K^+−solvent co-intercalation (i.e., graphite exfoliation).[143] Guo et al. reported that an anion-derived F-rich SEI was formed by tuning the solvation structure in the non-flammable and moderate-concentration electrolytes (i.e., KFSI/TMP, 3/8 in mol/mol) to control the decomposition path of the solvent and/or anion (i.e., less solvent decomposition), enabling a reversible K^+ (de)intercalation in graphite (Figure 8h).[135] Besides, the formation of an anion-derived SEI was induced by an anion-involved solvation structure in the concentrated electrolyte of 3.3 M KFSI in TMP, making the electrolyte compatible with the graphite.[134] Thus, herein a pendent viewpoint may be raised again, asking which factor, the solvation-structure-derived SEI or the solvation-structure-derived interfacial

https://doi.org/10.1021/acsenergylett.1c02425
ACS Energy Lett. 2022, 7, 490−513

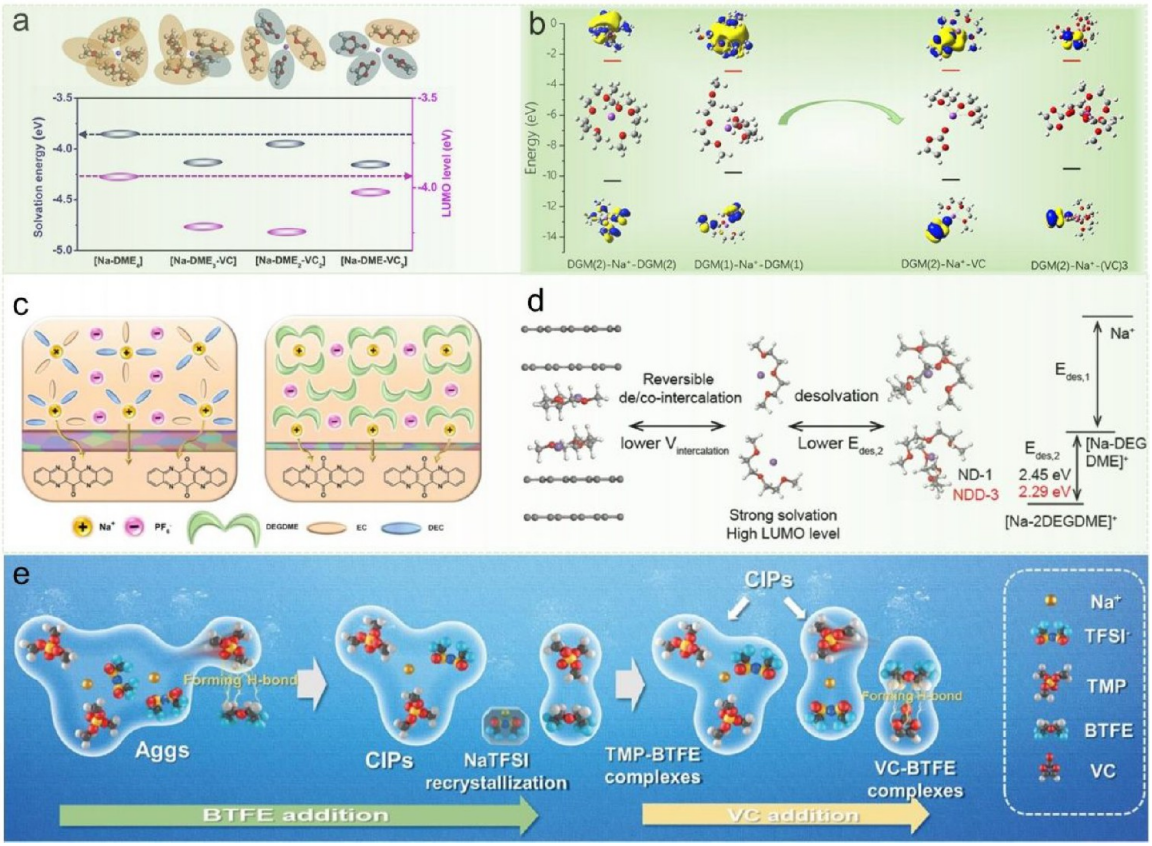

Figure 9. Improve electrode performance in SIBs by solvation structure effect. (a) Comparison of the calculated solvation energy and LUMO energy levels of the solvated complexes in the DME-based electrolytes with and without VC additive. (Reprinted with permission from ref 149. Copyright 2019 Elsevier.) (b) Adjusting the Na^+ solvation structure and the energy by VC additive. (Reprinted with permission from ref 150. Copyright 2021 Elsevier.) (c) Comparison of Na^+ solvation structures and interfacial behaviors on TAPQ electrode in EC/DEC and DEGDME-based electrolyte. (Reprinted with permission from ref 151. Copyright 2021 Wiley-VCH.) (d) Different desolvation energy of Na^+ solvation structure in the electrolyte of NDD-3 and ND-1 giving rise to different intercalated potentials. (Reprinted with permission from ref 152. Copyright 2021 Wiley-VCH.) (e) Tuning the Na^+ solvation structure by BTFE and VC in sequence. (Reprinted with permission from ref 153. Copyright 2021 Wiley-VCH.)

model, is dominant to determine graphite's performance in KIBs. A rigorous examination is required to further inspect the factors, and on account of the discussion in section 1, the exchange experiment for graphite electrode and electrolyte is believed to give more evidence.

4.2. Improve the Performance of Carbon and Other Anodes in Sodium-Ion Batteries by Solvation Structure Effect. The effect of solvation structure on improving the performance of hard carbon anodes has been also reported in sodium-ion batteries (SIBs).[144−148] For example, Bai et al. reported that VC additive tuned the solvation structure in DME-based electrolytes (i.e., 1.0 M $NaPF_6$, 0.5 vol% VC in DME) and lowered the LUMO energy levels of the VC-regulated solvation complexes (Figure 9a).[149] Then, a preferred decomposition occurred on the hard carbon anode to form a stable organic polymeric component-rich SEI, contributing a high capacity of 211 mAh g^{-1} over 2000 cycles at 1 A g^{-1}. In contrast, a fragile SEI was formed in the absence of the VC additive in the DME-based electrolytes and then led to a severe capacity decay. This role of the VC additive was further demonstrated in the electrolyte of 1.0 M $NaCF_3SO_3$ in diglyme (DGM) by Shi et al., where VC not only can change the Na^+ solvation sheath structure but also can assist to form an inorganic-rich SEI on an FeS@C anode.[150] This is because the LUMO level value of VC is lower than that of DGM, which promotes the change of the solvation sheath structure and the formation of the good SEI on the anode and thus leads to the prior reduction of VC (Figure 9b).

The solvation structure effects can be compared more clearly between the carbonate-based electrolytes and ether-based electrolytes.[151] It was found that a rigid solvation structure (e.g., $[Na^+(DEGDME)_x]$) was formed in the DEGDME-based electrolyte, leading to the formation of an inorganics-dominant SEI, which stabilized the *N*-heteropentacenequinone (TAPQ) anions and facilitated the multielectron redox reaction that occurred at different potentials. In comparison, a flexible solvation structure (e.g., $Na^+(EC/DEC)_y$) formed in the EC/DEC-based electrolyte to generate a thick SEI layer, due to the fact that the carbonate-based solvation sheath was unstable and prone to accept electrons due to the weak solvation energy and reduction stability (Figure 9c). In addition, it was reported that the DOL changed the Na^+ solvation structure in DEGDME-based electrolytes to obtain a high LUMO level for forming a thin and NaF-rich SEI on the graphite anode and also reducing the desolvation energy.[152] Compared to the value of 2.45 eV for 0.94 M $NaPF_6$ in DEGDME (ND-1), the value is reduced to 2.29 eV for 3.04 M $NaPF_6$ in DEGDME and DOL (10:1 by volume) (NDD-3), after the addition of DOL, which is expected to benefit the fractional solvent dissociation and inhibit the solvent co-intercalation, thereby lowering the

https://doi.org/10.1021/acsenergylett.1c02425
ACS Energy Lett. 2022, 7, 490−513

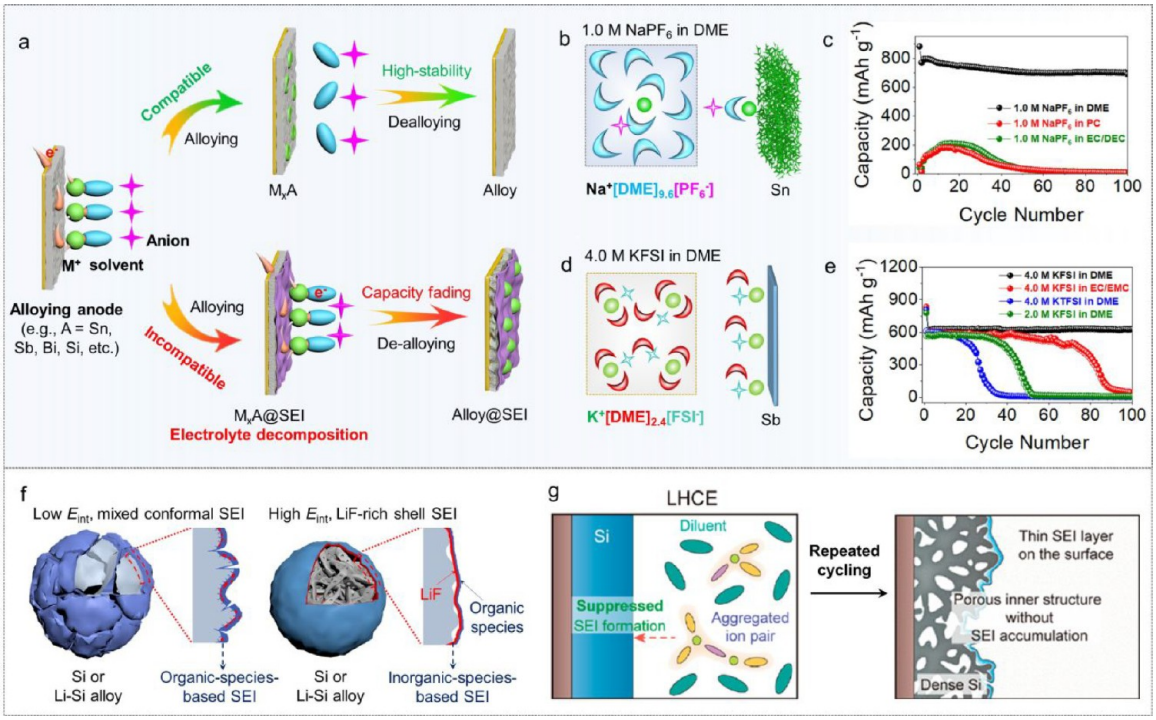

Figure 10. Design alloying-anode-compatible electrolyte in metal-ion batteries. (a) Competitive reaction pathways for M$^+$−solvent structure on the alloying anode. Optimized Na$^+$ and K$^+$ solvation structure, interfacial model, and performance for the (b, c) Sn and (d, e) Sb anode, respectively. (Reprinted with permission from ref 154. Copyright 2020 American Chemical Society. Reprinted with permission from ref 35. Copyright 2021 Wiley-VCH.) (f) Cycled alloying anode with low E_{int} and high E_{int} SEI induced by the different solvation structures in EC/DMC and mixTHF-based electrolyte, respectively. (Reprinted with permission from ref 164. Copyright 2020 Springer Nature.) (g) Regulating solvation structure in the OTE-based LHCE to form a thin SEI layer on the Si anode surface with a porous inner structure. (Reprinted with permission from ref 165. Copyright 2020 American Chemical Society.)

sodiation potential (Figure 9d). Besides, the effect of intermolecular H-bonds in the Na$^+$ solvation structure can be also regulated by the use of additives. Yang et al. demonstrated that BTFE molecules participated in the solvation shell of aggregates (AGGs) and repelled the TMP molecules out of the first solvation shell in the non-flammable electrolyte of 1.2 M NaTFSI-TMP/BTFE/VC, where the solvation balance between the Na$^+$ and TFSI$^-$ could be tuned by VC, giving rise to a VC-derived SEI layer on the hard carbon for high stability (e.g., high capacity retention of 99.6% after 100 cycles) (Figure 9e).[153] Although researchers have demonstrated the solvation structure effect for the improved performance, the reason was eventually ascribed to the solvation-structure-derived SEI that has good stability, which differs from the interpretation of the interfacial model and needs to be further examined by exchange experiments.

4.3. Design Alloying-Anode-Compatible Electrolyte in Metal-Ion Batteries. The proposed molecular interfacial model also provides a different view angle to study the performance of alloying anodes (e.g., Sn, Sb, Bi, etc.) in metal-ion batteries (i.e., M$^+$ = Li$^+$, Na$^+$, K$^+$).[35,154] Ming et al. presented two comparative interfacial reaction pathways for M$^+$−solvent−anion complex on the surface of alloying anodes (Figure 10a), where high performances can be expected if the M$^+$−solvent−anion complex in the interfacial model has good kinetics, thermodynamic properties, and electrochemical stability. Because of the difference from the graphite anode that there is no M$^+$−solvent co-intercalation into the alloying anode, it is requested to design stable electrolytes compatible with the alloying anode. It showed that the microsized Sn, Sb, or Bi alloying anodes were successfully stabilized in DME-based electrolytes, 1.0 M $NaPF_6$ (i.e., Na$^+$[DME]$_{9.6}$[PF$_6^-$]) or 1.0 M KPF_6 for SIBs and KIBs, respectively, while it was hard to achieve the same using other kinds of solvent (e.g., PC, EC/DEC, etc.) and salts (e.g., $NaCF_3SO_3$, $NaClO_4$) (Figure 10b,c). The bulk Sb anode was also stabilized in the DME-based electrolyte using 4.0 M KFSI (i.e., K$^+$[DME]$_{2.4}$[FSI$^-$]), where an extremely high capacity of 628 mAh g^{-1} (i.e., the value close to the theoretical capacity of K) and a good cycle performance of more than 100 cycles were obtained (Figure 10d,e). The high performance is hard to achieve once the solvent, salt, or concentration is changed. Thus, these results fully demonstrate the importance of the metal ion solvation structure and the properties of M$^+$−solvent−anion complexes in the interfacial model, where the ether-based electrolytes are more compatible with the alloying anodes without the need of alloying anode treatments, including carbon modification, structural designing, or SEI engineering.

The above findings indicate that the failure mechanism of the alloying anodes (e.g., severe capacity decay) may result from the incompatibility of electrolyte with the alloying anodes, which differs from the traditional viewpoint of electrode pulverization or the fracture of SEI.[155,156] Although studies showed that carbon modification,[157,158] nanostructure engineering,[159,160] and SEI engineering[122,161] could improve the stability and Coulombic efficiency of the alloying anodes, more and more researchers have demonstrated the importance of the solvation structure effect that can be tuned by electrolyte compositions (i.e., the species of salt, solvent, additives, concentration, etc.) to achieve high performances on alloying

https://doi.org/10.1021/acsenergylett.1c02425
ACS Energy Lett. 2022, 7, 490−513

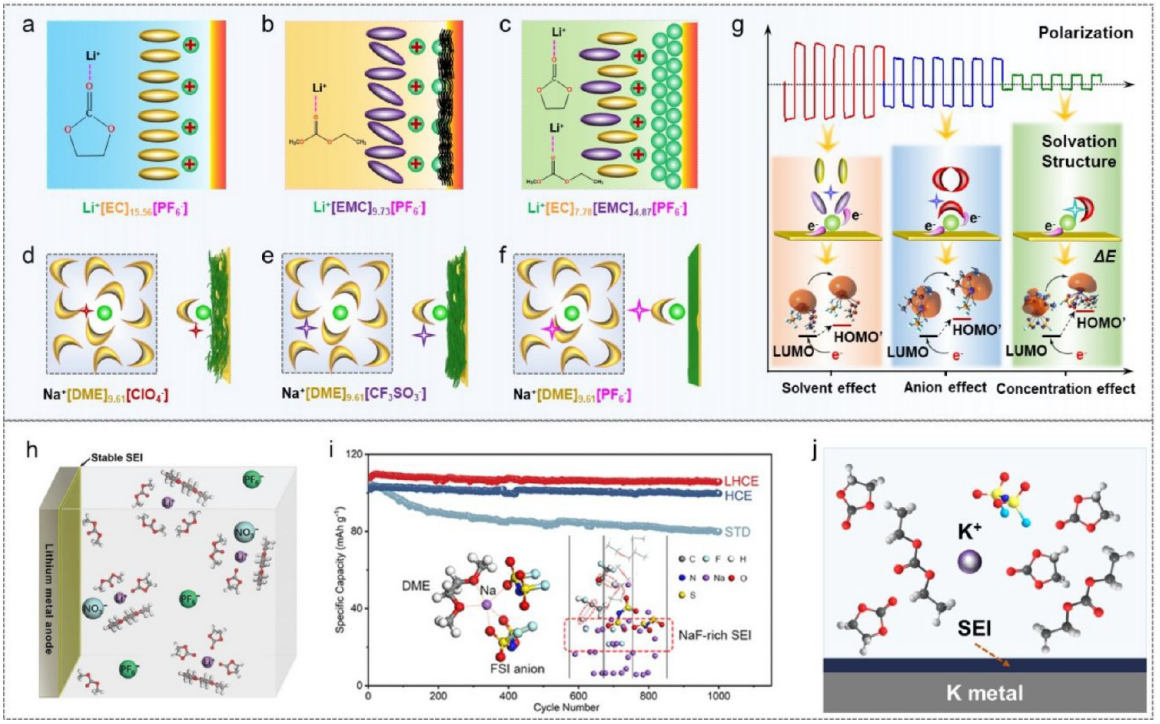

Figure 11. Design metal-anode-compatible electrolyte in metal batteries. (a–c) Interfacial model in EC, EMC, and EC/EMC-based electrolyte. (Reprinted with permission from ref 27. Copyright 2020 American Chemical Society.) Solvation structure and interfacial model of DME-based electrolyte using different metal salts of (d) $NaClO_4$, (e) $NaCF_3SO_3$, and (f) $NaPF_6$. (Reprinted with permission from ref 31. Copyright 2020 American Chemical Society.) (g) Effects of solvent, anion, and concentration on the interfacial model to turn the HOMO′/LUMO and the K plating/stripping behaviors. (Reprinted with permission from ref 30. Copyright 2020 American Chemical Society.) Solvation-structure-derived SEI regulated by (h) $LiNO_3$, (i) TTE, and (j) KFSI concentration for high metal plating/stripping performance in lithium, sodium, and potassium batteries, respectively. (Reprinted with permission from ref 179. Copyright 2020 Wiley-VCH. Reprinted with permission from ref 180. Copyright 2021 American Chemical Society. Reprinted with permission from ref 166. Copyright 2019 Wiley-VCH.)

anodes.[162,163] For example, Wang et al. reported that the contact ion pairs (CIPs) and AGGs in the solvation structure were dominant (i.e., >93%) in the electrolyte of 2.0 M $LiPF_6$ in tetrahydrofuran/2-methyltetrahydrofuran (mixTHF), facilitating the formation of a robust and LiF-rich SEI with a low adhesion (i.e., high interfacial energy (E_{int})) to the surface of the alloy, which improves the stability of the alloying anode (Figure 10f).[164] Zhang et al. designed an LHCE using 1*H*,1*H*,5*H*-octafluoropentyl 1,1,2,2-tetrafluoroethyl ether (OTE) as a diluent, in which the specific solvation structure with more AGGs helped to form a much thinner, more stable, and LiF-rich SEI layer, suppressing the continuous SEI growth, reducing the surface etching, and then giving rise to an excellent lithium storage capability (Figure 10g).[165] Further, Guo et al. studied the effects of salts (i.e., KFSI, KPF_6) and solvents (i.e., EC, DEC, DME) on the performance of the alloying anodes (e.g., red phosphorus, RP) in KIBs, where the solvation structure (i.e., 1.0 M KFSI in EC/DEC) was tuned to form a robust SEI on the K metal and RP electrode simultaneously to achieve a high performance (e.g., 440.2 mAh g^{-1}, high-capacity retention of 95% over 100 cycles).[166] The interpretations of the high performance of the alloying anodes in that research are ascribed again to the stable SEI that was derived from the solvation structure. However, the solvation structure may also change the interfacial model that makes the electrolyte compatible with the alloying anode. The exchange experiment is recommended to confirm which is the dominant factor that influences the alloying anode performance.

4.4. Design Metal-Anode-Compatible Electrolyte in Metal Batteries. More significant findings have been reported upon the study of the solvation structure and the interfacial model in battery systems using metallic anodes (M = Li, Na, K, etc.). For example, the solvation structure and interfacial model for the electrolytes employing 1.0 M $LiPF_6$ in EC (i.e., $Li^+[EC]_{15.56}[PF_6^-]$), EMC (i.e., $Li^+[EMC]_{9.73}[PF_6^-]$), and EC/EMC (i.e., $Li^+[EC]_{7.78}[EMC]_{4.87}[PF_6^-]$) were compared to understand the different lithium plating phenomena.[27] It is hard to plate Li on the Cu foil in EC electrolyte due to the strong Li^+-EC interaction (Figure 11a), while a severe electrolyte decomposition occurred in EMC electrolyte due to the instability of Li^+-EMC (vs Li^+-EC) (Figure 11b). These phenomena are observed as well in other kinds of electrolytes when linear carbonates (e.g., DMC, DEC) are used as the single solvent. In contrast, in the EC/DEC-based electrolyte, EC can occupy the surface of the electrode due to the stronger Li^+-EC interaction (vs Li^+-EMC), while EMC prefers to distribute behind EC molecules, forming a regular zigzag structure (Figure 11c). Then, Li^+ could be desolvated readily and plated on the electrode due to the weakened interaction of Li^+-EC by EMC, and meanwhile EMC could be also stabilized because it appears as free molecules that are far from Li^+ without any polarization. This interpretation is similar to that explaining why EC/DEC-based electrolytes are compatible with the graphite electrode while EC or DEC electrolytes are

https://doi.org/10.1021/acsenergylett.1c02425
ACS Energy Lett. 2022, 7, 490–513

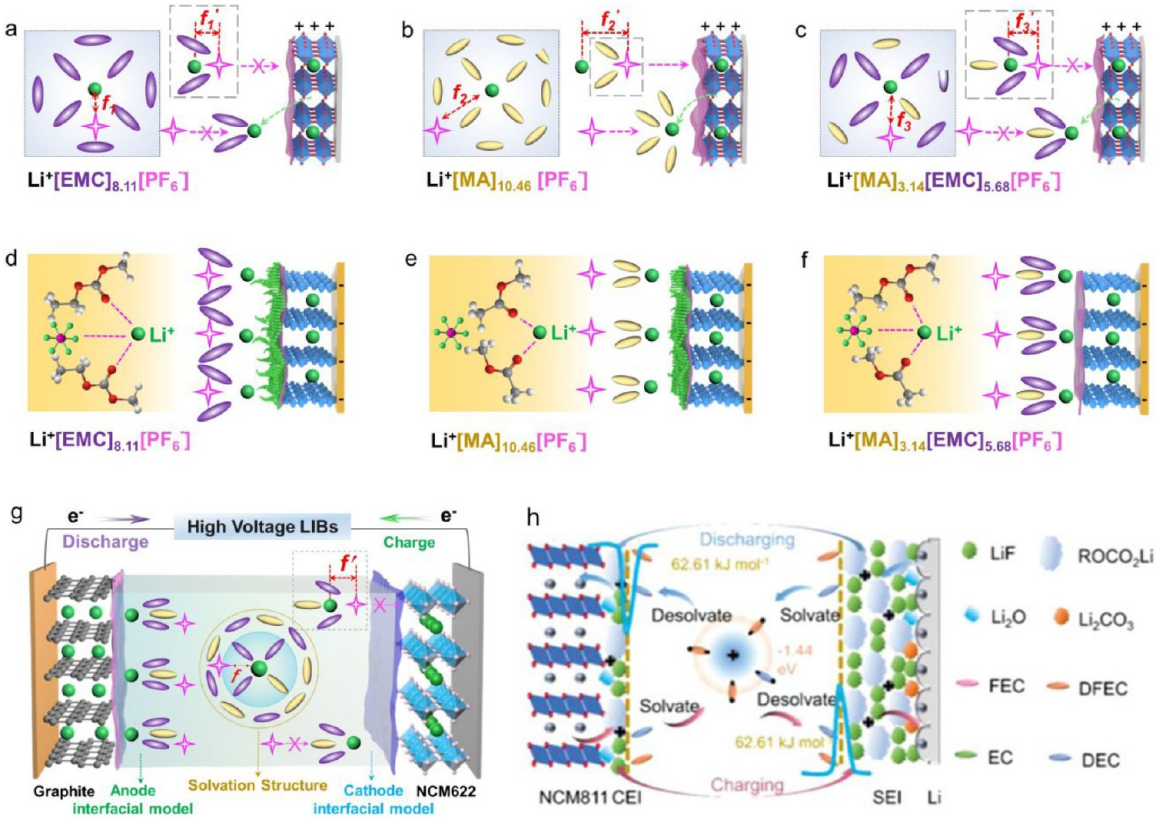

Figure 12. Construct the cathode interfacial model and design cathode/anode-compatible electrolyte. Cathode and anode interfacial models in (a, d) EMC, (b, e) MA, and (c, f) EMC/MA-based electrolyte. (Reprinted with permission from ref 36. Copyright 2021 Wiley-VCH.) (g) Solvation structure and multi-interfacial behaviors on the NCM622 cathode and graphite anode simultaneously in lithium-ion full battery. (h) Schematic of the dynamic evolution of the Li^+ solvation sheath in the NCM811|Li cell during the charging/discharging process in the 1.0 M $LiPF_6$ in DFEC/DEC electrolyte. (Reprinted with permission from ref 189. Copyright 2021 Wiley-VCH GmbH.)

incompatible, as discussed earlier (Figure 7b).[25] This interfacial model is applicable to interpreting the lithium deposition process in a broad electrolyte system.[167]

Besides, the most commonly used EC has also been discovered to have another important role in stabilizing electrolytes,[27] besides its well-known roles of dissociating lithium salts and forming an SEI. Thus, although recently many researchers have focused on designing EC-free electrolytes to avoid its oxidation on the cathode side,[168−170] we have to keep this issue in mind that a stable interfacial model (i.e., good dynamic and electrochemical stability of Li^+−solvent−anion complex) needs to be achieved by tuning the electrolyte compositions prudently. Otherwise, a severe capacity decay could be observed when the EC solvent is absent. Moreover, improving the electrochemical stability of Li^+−solvent−anion in the interfacial model becomes even more important in negative-electrode-free lithium metal batteries.[171−173] This is because the current collector and/or metal's capacity for electron-donation to the Li^+−solvent−anion complex is much higher than that of the normal anode (i.e., carbon-based anode), in turn decreasing the electrolyte's stability and also adding complexities in electrolyte decomposition and lithium dendrite growth.

In addition, an anion-based interfacial model has been built by Ming et al. to guide the design of electrolytes that are compatible with Na plating/stripping,[27] where anion-induced corrosion has been demonstrated to be the main reason for the failure and low CE of sodium batteries. It was found that the ClO_4^- and $CF_3SO_3^-$ are close to the interface of the Na metal due to the low steric hindrance of ClO_4^- or the strong interaction between $CF_3SO_3^-$ and Na^+, causing a serious electrolyte decomposition and thereby a low CE. In contrast, the PF_6^- is located far from the electrode interface in the DME-based electrolyte (i.e., $Na^+[DME]_{9.61}[PF_6^-]$), leading to high reversibility of the Na plating/stripping process (Figure 11d−f). Notably, the high value of ΔE (i.e., HOMO′/LUMO, 0.0493 hartree) for Na^+-DME-PF_6^- is also responsible for the high stability of electrode performances.[31] Based on the interfacial model, an electrolyte compatible with potassium metal has also been designed by changing the kind of solvent, salt, and concentration, in which the kinetics, thermodynamic properties, and electrochemical stability of the K^+−solvent−anion could be tuned accurately, achieving a low polarization and high Coulombic efficiency in potassium batteries (Figure 11g). The interfacial model can well interpret why the electrolyte of 5.0 M KFSI in DME (i.e., $K^+[DME]_{1.92}[FSI^-]$) is optimal for potassium batteries.[30]

The solvation-structure-derived interfacial model can give reasonable interpretations for the different battery performances, while other viewpoints believe that the high performances result from the solvation-structure-derived SEI that has good stability.[166,174−178] For example, a highly conductive LiN_xO_y-containing SEI was formed on the electrode surface by regulating the solvation structure using $LiNO_3$ additive in TEGDME-based electrolyte, enabling dendrite-free lithium deposition even under a high-capacity operating condition of 4

https://doi.org/10.1021/acsenergylett.1c02425
ACS Energy Lett. 2022, 7, 490−513

mAh cm^{-2} (Figure 11h).[179] Additionally, Xiang et al. reported that a NaF-rich SEI was formed on the Na anode surface when TTE was added into 3.8 M NaFSI/DME electrolyte to form an LHCE, as the formed Na^+-1DME-2FSI^- solvation structure led to the decomposition of more FSI^- with less DME decomposition, enabling a high capacity retention of 98.4% after 1046 cycles at 2C in a Na||$Na_3V_2(PO_4)_3$ (NVP) cell (Figure 11i).[180] Moreover, Guo et al. found that a robust and flexible organic−inorganic SEI layer can be formed in the electrolyte with the low LUMO energy (i.e., 1.0 M KFSI/EC + DEC), where the EC/DEC mixed solvents and FSI are more easily decomposed, enabling fast K^+ ion diffusion/desolvation for better potassium metal protection and cycling stability (Figure 11j).[166] However, these studies partially emphasize that the good stability of the solvation-structure-derived SEI contributes to the high metal anode performance but fail to take the interfacial behavior of the solvation structure into consideration, which can rationally illustrate the different performances observed in different electrolytes, as interpreted by Ming et al. earlier in this section.

In stark contrast, some researchers have realized the significance of M^+ solvation structure and the interfacial behaviors to improve the battery performance.[167,181−183] For example, Liu et al. found that the balance between cation−solvent and cation−anion in the solvation shell was even more important for stabilizing lithium metal anodes compared to the SEI.[174] In the 1.0 M LiFSI in DOL/DME system, the local charge-transfer impedance increased largely and the binding energy of $Li^+(DME)_{2.3}$ was as high as −414 kJ mol^{-1} in the ultralow temperature environment (e.g., −40/−60 °C), resulting in tip-driven manner kinetics of the Li deposition and the eventual generation of Li dendrites. In contrast, in the 1.0 M LiFSI in diethyl ether (DEE) system, the binding energy of $Li^+(DEE)_{1.8}$ (−280 kJ mol^{-1}) is weak, thus resulting in a uniform Li deposition. In this case, all these results have considered the effects of solvation structure, demonstrating the importance of the solvation structure in metal batteries. However, whether the solvation-structure-derived interfacial model or SEI, which one is the dominant factor for the performance needs to be well considered.

4.5. Construct the Cathode Model and Design Cathode/Anode-Compatible Electrolyte in Lithium-Ion Full Batteries. Although the effect of the solvation structure and particularly the interfacial model on the anode performance has been studied since 2018,[24] there was no report paying attention to the interfacial model on the cathode side until 2021.[36] This is because many efforts focused on tuning the electrolyte compositions to improve the cathode stability by forming a stable cathode electrolyte interface (CEI), which is believed to suppress the electrolyte decomposition and electrode degradation, specifically in the high voltage conditions (i.e., >4.3 V vs Li/Li^+).[177,184−186] For example, Xue et al. designed a sulfonamide-based electrolyte (i.e., 1.0 M LiFSI in *N,N*-dimethyltrifluoromethanesulfonamide (DMTMSA)) to ensure the $LiNi_{0.8}Co_{0.1}Mn_{0.1}O_2$ (NCM811) cycled stably at 4.7 V by forming a LiF-like inorganic CEI.[187]

Besides designing the CEI, a new interfacial model of the cathode was presented recently to show how Li^+, anions, and solvents interact and influence the cathode's performance in the cases of EMC (i.e., $Li^+[EMC]_{8.11}[PF_6^-]$), methyl acetate (MA) (i.e., $Li^+[MA]_{10.46}[PF_6^-]$), and EMC/MA-based electrolytes (i.e., $Li^+[MA]_{3.14}[EMC]_{5.68}[PF_6^-]$).[36] It was found that PF_6^- has a high frequency (i.e., f_1) that appears around Li^+ in the solvation structure in the EMC-based electrolyte due to the low dielectric constant of EMC (i.e., ε = 2.958), and then a strong interaction (i.e., f_1') exists between Li^+ and EMC-PF_6^-. Such a strong interaction weakens the Coulombic interaction between PF_6^- and the positively charged cathode (Figure 12a), enabling the EMC-PF_6^- pair to keep far from the cathode surface and then avoid its oxidation. Besides, the oxidation stability of free EMC solvent molecules is also improved, because the free EMC can coordinate with Li^+ to form a Li^+-EMC pair when Li^+ is extracted from the cathode upon the charging process. More importantly, PF_6^- is also difficult to be desolvated in the initial Li^+ solvation structure to move close to the "newly" formed Li^+-EMC pair. Thus, the detrimental effect of PF_6^- that reacts with EMC solvent to produce HF could be maximally mitigated.

In contrast, in the MA electrolyte, PF_6^- has a low frequency that appears around Li^+ (i.e., f_2) in the solvation structure due to the high dielectric constant of MA (vs EMC) (i.e., ε = 6.68) (Figure 12b), and then a weak interaction exists between the MA-PF_6^- pair and Li^+ (i.e., f_2'). Thus, MA-PF_6^- moves closer to the cathode surface due to the strong Coulombic interaction between the PF_6^- and the positively charged cathode, making the electron transfer from MA-PF_6^- to the cathode easier and thus leading to a lower oxidation stability of MA-PF_6^-. The oxidation stability of the free MA solvent cannot be improved, because the PF_6^- can be desolvated from the initial Li^+ solvation structure readily and then move closer toward the newly formed Li^+-MA pair. Fortunately, in the E/M73 electrolyte (i.e., 1.2 M LPF_6 in EMC/MA (7/3 in v/v), $Li^+[MA]_{3.14}[EMC]_{5.68}[PF_6^-]$), PF_6^- has a medium frequency (i.e., f_3) that appears around Li^+ (Figure 12c), and thus a medium interaction exists between the Li^+−solvent and PF_6^-. In this way, a safe distance can be maintained between the PF_6^- and the positively charged cathode owing to the medium Coulombic interaction, giving rise to a high oxidation stability of the E/M73 electrolyte.

Besides the cathode side, Ming et al. also constructed the corresponding interfacial model on the anode side. For example, in the EMC electrolyte, the high binding energy of Li^+-EMC results in a difficult desolvation, and then the resultant high polarization causes the growth of lithium dendrites on the graphite anode (Figure 12d). In the MA electrolyte, the lithium could be plated due to the low desolvation energy of Li^+-MA, but MA that is close to the anode surface can react with lithium metal easily (Figure 12e). In the EMC/MA-based electrolyte, the Li^+-EMC is weakened by MA solvent, while the PF_6^- could also keep far from Li^+ compared to that in the EMC electrolyte (Figure 12f). Then, Li^+ desolvation becomes easier, and the intercalation of Li^+ into the graphite anode is preferable compared to the formation of lithium dendrites. Finally, Ming et al. have not only built a new interfacial model on the cathode side for the first time but also constructed the dynamic mutual interaction interfacial behavior on the cathode and anode simultaneously in a battery to interpret the battery's performance (Figure 12g). The presented interfacial model enables us to interpret the reason why regulating the solvent-depleted electrolyte with metal−organic framework (MOF) materials could suppress the electrolyte decomposition/side reactions on the cathode.[188] Besides, we believe that the high capacity and stability of the NCM811|Li cell can be also interpreted by different cathode interfacial models when the difluoroethylene (DFEC)-based electrolyte was compared to ethylene carbonate (EC)- and

https://doi.org/10.1021/acsenergylett.1c02425
ACS Energy Lett. 2022, 7, 490−513

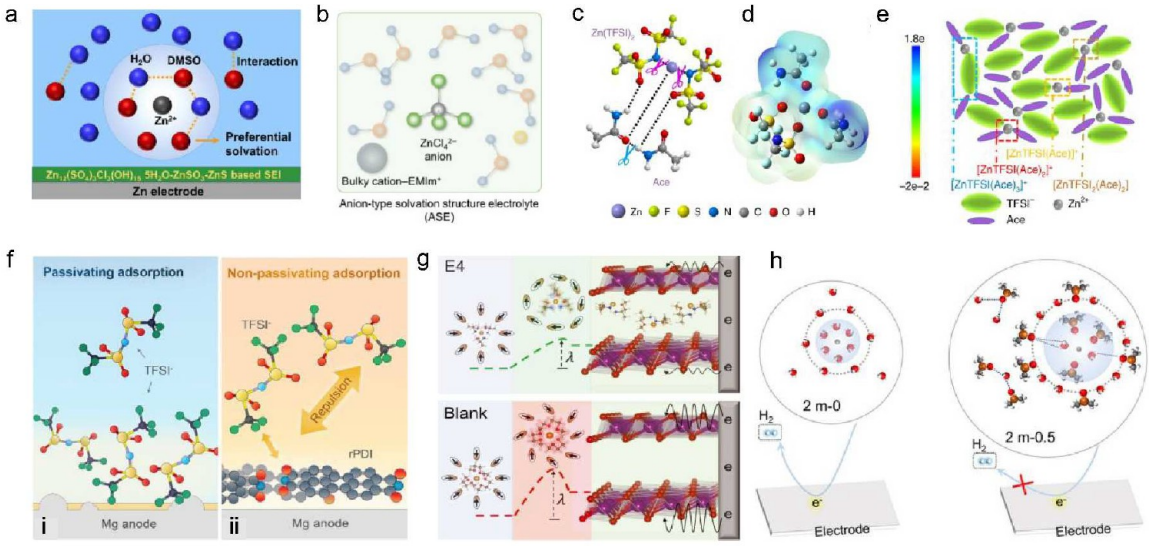

Figure 13. Improve polyvalent ion batteries' performance and beyond by solvation effect. (a) Modulated Zn^{2+} solvation structure and surface passivation in $ZnCl_2$ aqueous electrolyte by adding DMSO. (Reprinted with permission from ref 191. Copyright 2020 American Chemical Society.) (b) Anion-type water-free Zn^{2+} solvation structure. (Reprinted with permission from ref 194. Copyright 2021 Wiley-VCH.) (c) Schematic diagram of the interplay among Zn^{2+}, $TFSI^-$, and acetamide (Ace) to form eutectic solutions. (d) Molecular electrostatic potential energy surface of $[ZnTFSI(Ace)_2]^+$. (e) Illustration of the representative environment of active Zn species within the $Zn(TFSI)_2$-based eutectic solvent. (Reprinted with permission from ref 190. Copyright 2020 Springer Nature.) (f) Passivating and non-passivating adsorption of $TFSI^-$ on the Mg anode. (Reprinted with permission from ref 198. Copyright 2021 American Chemical Society.) (g) Reorganizing the Mg^{2+} solvation sheath in the 0.5 M $Mg(TFSI)_2$ in DME−1-methoxy-2-propylamine electrolyte to concert the ion and electron transfer in the $Mg_{0.15}MnO_2$ cathode. (Reprinted with permission from ref 197. Copyright 2021 The American Association for the Advancement of Science.) (h) Regulating the Zn^{2+} solvation structure in $NaClO_4/H_2O$ electrolyte by DMSO to inhibit the HER. (Reprinted with permission from ref 204. Copyright 2021 American Chemical Society.)

fluoroethylene (FEC)-based electrolytes (Figure 12h).[189] The success of constructing the interfacial model on cathodes and anodes and studying their interactions opens a new avenue to understand battery performance from the molecular scale, besides the CEI and SEI concepts.

4.6. Improve the Performance of Polyvalent Ion Batteries and Beyond by Solvation Effect. The solvation effect is being widely studied in polyvalent ion batteries (e.g., Zn^{2+},[190−194] Mg^{2+},[195−199] Ca^{2+},[200,201] Al^{3+}[202,203]) and other fields such as electrocatalysis.[204−206] This research trend was promoted in 2018 by Ming et al., based on their viewpoint that the solvation structure and interfacial model (vs SEI) can influence the electrode's performance significantly.[24−26] For example, DMSO replaced H_2O in the first Zn^{2+} solvation sheath in $ZnCl_2-H_2O$ electrolyte and then effectively suppressed H_2O decomposition; meanwhile, the modified solvation structure induced the formation of an inorganic-rich SEI on zinc to guarantee a high CE and a long cycle life over 500 cycles (Figure 13a).[191] This viewpoint was further demonstrated by introducing a bulky cation (e.g., 1-ethyl-3-methylimidazolium chloride) into $ZnSO_4-H_2O$ electrolyte to construct an anion-type water-free solvation structure, $ZnCl_4^{2-}$, in order to drive water out of the $Zn(H_2O)_6^{2+}$ solvation structure and then suppress Zn dendrite growth and hydrogen evolution reaction (HER) (Figure 13b).[194] In addition, a new kind of eutectic solvent based on acetamide and $Zn(TFSI)_2$ was designed by Cui et al., where $TFSI^-$ coordinated with Zn^{2+} to form an anion-containing Zn complex (i.e., $[ZnTFSI_m(Ace)_n]^{(2-m)+}$), leading to a preferential reductive decomposition of $TFSI^-$ before Zn deposition.[190] Then, an anion-derived SEI layer rich in mechanically rigid ZnF_2 and Zn^{2+}-permeable organic (e.g., S and N) components was formed, enabling the long-term cycling of dendrite-free zinc plating/stripping reactions (>2000 cycles, high CE of 99.7%) (Figure 13c−e).

Regulating the solvation structure and interfacial model could also improve the Mg plating/stripping process, addressing the major challenge of severe capacity decay in magnesium-ion batteries (MIBs). For example, the perylene diimide−ethylene diamine (rPDI) additive in the electrolyte of $Mg(TFSI)_2$-$MgCl_2$ in DME exhibited higher adsorption energy than that of $TFSI^-$ on Mg electrode surface, preventing the decomposition of $TFSI^-$ and passivation of Mg anode (Figure 13f).[198] In addition, Wang et al. found that adding methoxyethylamine chelates with a high affinity into the DME-based electrolytes (e.g., 0.5 M $Mg(TFSI)_2$) not only promoted the interfacial charge-transfer kinetics but also suppressed the side reactions on the electrode surface.[197] This is because the chelant-rich solvation sheaths bypass the energetically unfavorable desolvation process through reorganization, thus reducing the overpotential and suppressing the concomitant parasitic reactions for both the anode and the cathode in MIBs (Figure 13g). Likewise, a similar method and results were also validated in calcium-ion batteries. For example, regulating the Ca^{2+} solvation structure by adding 1-methoxy-4-butylamine (M4B) to 0.5 M calcium tetrabis-(hexafluoroisopropyloxy)borate−DME electrolyte enhanced the CE of Ca plating/stripping to 96%.[197]

Besides the solvation structure in bivalent cations, a "water-in-salt" aqueous electrolyte ($AlCl_3·6H_2O$) in aqueous aluminum-ion batteries (AIBs) was also proposed to decrease the number and activity of free H_2O significantly by Leung et al., where the electrochemical stability window was expanded to 4 V with a high capacity of 165 mAh g^{-1} at 500 mA g^{-1} and a long lifespan of over 1000 cycles in the full aluminum-ion

https://doi.org/10.1021/acsenergylett.1c02425
ACS Energy Lett. 2022, 7, 490−513

battery.[202] However, very few researchers reported the Al^{3+} solvation structure due to the high ion valence and relatively large ion radius of Al^{3+}, the effects of which can be additionally studied. Note that the effect of the solvation structure can be further applied in the field of electrocatalysis and beyond. For example, Chen et al. found that DMSO directly entered the Na^+ solvation sheath, replaced part of the coordinated water molecules, and also bonded to all the hydrogen atoms in water molecules in the DMSO−H_2O H-bond network after the DMSO was added into $NaClO_4$−H_2O electrolytes (Figure 13h).[204] In this way, the activity of water molecules was reduced, thus suppressing the HER side reactions effectively and expanding the HER potential from 0.6 to 1.6 V (vs Ag/AgCl with saturated KCl). Herein, although greater performances have been achieved by tuning the solvation structure, most interpretations are conventionally ascribed to the solvation-structure-derived SEI that has good stability. We would like to emphasize that more efforts need to be dedicated to the study of the solvation-structure-derived interfacial model, since the cation desolvation step can also affect the performance. In many cases, the effect of the interfacial model may be dominant, as summarized in the above sections.

5. Summary and Outlook. The effects of metal-ion solvation structure and the interfacial model on battery performances have been summarized in this Focus Review from the initial discovery, through the rapid development, to the growing interest in the concept, which is expected to become the mainstream research trend. Many unexplained phenomena in electrode performance are rationally interpreted from the aspects of the solvation structure and the derived interfacial model (i.e., metal ion desolvation process), which complements the traditional SEI and CEI interpretation well. The knowledge of the SEI contributed significantly to the rapid development of LIBs, particularly the electrolyte design in the past two decades, and many researchers continue to focus on characterizing and engineering the SEI, as well as its relationship with the electrolyte compositions and electrode performance, aiming to further improve the LIBs' performances in safety, energy density, and life-span.

However, the discovered dominant roles of the solvation structure and interfacial model for the electrode performance simulate researchers to reconsider the known effect of the SEI. In other words, we may have already entered a new era of solvation structure and interfacial models—i.e., a post-SEI era—since this knowledge can help researchers to understand the electrolyte and its behaviors on the electrode surface at the molecular level. Many more scientific connections can be built between the solvation-structure-derived interfacial model and electrode performance, following which the electrolyte can be designed more effectively and the electrode's performance can be predicted. Although the effects of solvation structure and interfacial model are being verified by changing the electrolyte decompositions, most of the interpretations are based on schematic illustrations for the electrolyte microstructure and desolvation behaviors, which require further convincing characterizations. This is a complex research topic since it involves the solution, electrochemistry, and interfacial chemistry at least, but these theories are significant as they are needed in many fields to analyze electrolyte performance once the electrolyte−electrode interface exists. Thus, many scientific problems need to be addressed to promote the development of the solvation structure and interfacial model.

(i) Analyzing quantitatively the solvation structure and the dynamic desolvation process. The basic parameters of a single solvation structure (e.g., coordination number, bond length, angle, etc.) and the interactions between the neighboring solvation structures (e.g., long-range solvent−solvent and solvent−anion interactions) need to be characterized since they can shape the electrolyte's properties. The dynamic metal ion (de)solvation process on the electrode interface also needs to be analyzed by *in situ* spectroscopy, theoretical simulation, and quantum chemistry calculation. Empirical parameters, formula, force field, and so forth need to be constructed to build the relationship between the (de)solvation behaviors and battery performance. Moreover, thermodynamic data of the solvent, salt, and electrolyte (e.g., M^+−solvent−anion complex) need to be studied and supplemented, making it a scientific knowledge that can be reproduced, quantified, and learned.

(ii) Balancing the interfacial model of the cathode and the anode. The metal-ion (de)solvation process on the cathode and the anode surface occurs simultaneously, but the reaction is opposite (i.e., oxidation vs reduction), which can affect the electrolyte stability and battery performance. The criteria of choosing the appropriate kind of solvent, metal salt, and concentration need to be developed to balance the oxidation−reduction reaction and the (de)solvation process at the cathode and anode interface simultaneously. Besides, the interaction between the cathode and anode interfacial models needs to be clarified based on the full-cell performance, guiding the design of electrolytes compatible with the cathode and anode maximally.

(iii) Combining the effect of solvation structure and the SEI. Significant attention needs to be paid to elucidate the effects of SEI and CEI, since the solvation structure effect has been proved. The CEI and SEI may expand the electrochemical window of the electrolyte and then improve the electrolyte stability (e.g., chemical stability of M^+−solvent−anion complex). This viewpoint needs to be further verified by experiments. Building the scientific connections between the SEI, solvation structure effect, interfacial model, and the electrode's performance is essential to design electrolytes and improve battery performance more effectively.

(iv) Exploring the solvation structure effect and the interfacial model in the next generation of lithium−sulfur (Li-S) and lithium−oxygen (Li-O_2) batteries. Besides the effect on lithium metal electrode as discussed above, the Li^+ solvation structure can be altered by the dissolution of lithium polysulfides (Li_2S_x, $2 < x \leq 8$) in Li-S batteries, while the electrode−electrolyte (solid−liquid) interfacial behaviors can also be changed by oxygen in Li-O_2 batteries. The relationship between the changed Li^+ solvation structure, interfacial model, and battery performance needs to be further investigated since we have demonstrated their influences in metal-ion and metal batteries.

Briefly, besides the SEI effect, understanding the effects of solvation structure and interfacial model (i.e., (de)solvation process) can guide functional electrolyte design more effectively to improve LIB performances and particularly satisfy the need for LIBs with high voltage, fast charging,

https://doi.org/10.1021/acsenergylett.1c02425
ACS Energy Lett. 2022, 7, 490−513

wide operating temperature range, and so forth to be competent for specific working conditions. Thus, a new era is coming that could contribute to the rapid development of LIBs and beyond from a different perspective.

AUTHOR INFORMATION

Corresponding Authors

Qian Li − *State Key Laboratory of Rare Earth Resource Utilization, Changchun Institute of Applied Chemistry, Chinese Academy of Sciences, Changchun 130022, China*; Email: qianli@ciac.ac.cn

Jun Ming − *School of Applied Chemistry and Engineering, University of Science and Technology of China, Hefei 230026, China; State Key Laboratory of Rare Earth Resource Utilization, Changchun Institute of Applied Chemistry, Chinese Academy of Sciences, Changchun 130022, China*; orcid.org/0000-0001-9561-5718; Email: jun.ming@ciac.ac.cn

Authors

Haoran Cheng − *State Key Laboratory of Rare Earth Resource Utilization, Changchun Institute of Applied Chemistry, Chinese Academy of Sciences, Changchun 130022, China; School of Applied Chemistry and Engineering, University of Science and Technology of China, Hefei 230026, China*

Qujiang Sun − *State Key Laboratory of Rare Earth Resource Utilization, Changchun Institute of Applied Chemistry, Chinese Academy of Sciences, Changchun 130022, China*

Leilei Li − *State Key Laboratory of Rare Earth Resource Utilization, Changchun Institute of Applied Chemistry, Chinese Academy of Sciences, Changchun 130022, China*

Yeguo Zou − *State Key Laboratory of Rare Earth Resource Utilization, Changchun Institute of Applied Chemistry, Chinese Academy of Sciences, Changchun 130022, China; School of Applied Chemistry and Engineering, University of Science and Technology of China, Hefei 230026, China*

Yuqi Wang − *State Key Laboratory of Rare Earth Resource Utilization, Changchun Institute of Applied Chemistry, Chinese Academy of Sciences, Changchun 130022, China; School of Applied Chemistry and Engineering, University of Science and Technology of China, Hefei 230026, China*

Tao Cai − *State Key Laboratory of Rare Earth Resource Utilization, Changchun Institute of Applied Chemistry, Chinese Academy of Sciences, Changchun 130022, China; School of Applied Chemistry and Engineering, University of Science and Technology of China, Hefei 230026, China*

Fei Zhao − *State Key Laboratory of Rare Earth Resource Utilization, Changchun Institute of Applied Chemistry, Chinese Academy of Sciences, Changchun 130022, China; School of Applied Chemistry and Engineering, University of Science and Technology of China, Hefei 230026, China*

Gang Liu − *State Key Laboratory of Rare Earth Resource Utilization, Changchun Institute of Applied Chemistry, Chinese Academy of Sciences, Changchun 130022, China; School of Applied Chemistry and Engineering, University of Science and Technology of China, Hefei 230026, China*

Zheng Ma − *State Key Laboratory of Rare Earth Resource Utilization, Changchun Institute of Applied Chemistry, Chinese Academy of Sciences, Changchun 130022, China*

Wandi Wahyudi − *Physical Science and Engineering Division, King Abdullah University of Science and Technology, Thuwal 23955-6900, Saudi Arabia*; orcid.org/0000-0002-6224-2414

Complete contact information is available at: https://pubs.acs.org/10.1021/acsenergylett.1c02425

Author Contributions

†H.C. and Q.S. contributed equally to this work.

Notes

The authors declare no competing financial interest.

Biographies

Haoran Cheng is currently pursuing his Ph.D. degree at the School of Applied Chemistry and Engineering, University of Science and Technology of China. His primary research interests include electrolyte design and electrode interfacial analysis.

Qujiang Sun obtained his Ph.D. in applied chemistry from the University of Chinese Academy of Sciences in 2019. His current research interest focuses on electrode and electrolyte design.

Leilei Li obtained his Ph.D. in chemical technology from China University of Mining and Technology, Beijing, in 2021. His current research interest focuses on aqueous electrolyte design.

Yeguo Zou is currently pursuing his Ph.D. degree at the School of Applied Chemistry and Engineering, University of Science and Technology of China. His research focuses on high-voltage electrolyte design and dynamic analysis of the electrode/electrolyte interface.

Yuqi Wang is currently pursuing his M.S. degree at the School of Applied Chemistry and Engineering, University of Science and Technology of China. His primary research interests include metal-compatible electrolyte design and electrode interface analysis.

Tao Cai is currently pursuing his M.S. at the School of Applied Chemistry and Engineering, University of Science and Technology of China. His primary research interests include anode-compatible electrolyte design and electrode interfacial analysis.

Fei Zhao is currently pursuing his M.S. degree at the School of Applied Chemistry and Engineering, University of Science and Technology of China. His primary research interests include anode-compatible electrolyte design and electrode interfacial analysis.

Gang Liu is currently pursuing his Ph.D. degree at the School of Applied Chemistry and Engineering, University of Science and Technology of China. His primary research interests include the electrolyte and electrode interface for alkali-metal-ion batteries.

Zheng Ma obtained her Ph.D. degree from the School of Chemistry, Monash University, Australia, in 2018. Her research interests include energy storage devices.

Wandi Wahyudi obtained his Ph.D. in materials science and engineering from King Abdullah University of Science and Technology in 2021. His current research interest focuses on electrolyte design.

Qian Li obtained her Ph.D. in applied chemistry from the University of Science and Technology of China in 2020. Then, she became a research assistant at the Changchun Institute of Applied Chemistry, Chinese Academy of Sciences. Her primary research interests include the electrolyte and electrode interfaces for metal-ion batteries.

Jun Ming obtained his Ph.D. from the Changchun Institute of Applied Chemistry, Chinese Academy of Sciences. He became a full professor at the Changchun Institute of Applied Chemistry, Chinese Academy of Sciences, in 2017. His primary research interests include the electrolyte design and electrode interfacial model for metal-ion and metal−sulfur batteries.

https://doi.org/10.1021/acsenergylett.1c02425
ACS Energy Lett. 2022, 7, 490−513

■ ACKNOWLEDGMENTS

The authors greatly thank the National Natural Science Foundation of China (22122904) for funding support. This work is also supported by the National Natural Science Foundation of China (21978281, 22109155) and the Scientific and Technological Developing Project of Jilin Province (YDZJ202101ZYTS022). The authors also thank the Independent Research Project of the State Key Laboratory of Rare Earth Resources Utilization (110005R086), Changchun Institute of Applied Chemistry.

■ REFERENCES

(1) Tarascon, J. M.; Armand, M. Issues and Challenges Facing Rechargeable Lithium Batteries. *Nature* **2001**, *414*, 359−367.
(2) Scrosati, B.; Hassoun, J.; Sun, Y. K. Lithium-ion Batteries. A Look into the Future. *Energy Environ. Sci.* **2011**, *4*, 3287−3295.
(3) Li, M.; Lu, J.; Chen, Z.; Amine, K. 30 Years of Lithium-Ion Batteries. *Adv. Mater.* **2018**, *30*, e1800561.
(4) Wu, Y.; Xie, L.; Ming, H.; Guo, Y.; Hwang, J. Y.; Wang, W.; He, X.; Wang, L.; Alshareef, H. N.; Sun, Y. K.; Ming, J. An Empirical Model for the Design of Batteries with High Energy Density. *ACS Energy Lett.* **2020**, *5*, 807−816.
(5) Mogi, R.; Inaba, M.; Jeong, S. K.; Iriyama, Y.; Abe, T.; Ogumi, Z. Effects of Some Organic Additives on Lithium Deposition in Propylene Carbonate. *J. Electrochem. Soc.* **2002**, *149*, A1578.
(6) Xu, K. Nonaqueous Liquid Electrolytes for Lithium-Based Rechargeable Batteries. *Chem. Rev.* **2004**, *104*, 4303−4418.
(7) Zhang, S. S. A Review on Electrolyte Additives for Lithium-Ion Batteries. *J. Power Sources* **2006**, *162*, 1379−1394.
(8) Zhang, S. S.; Xu, K.; Jow, T. R. Enhanced Performance of Li-Ion Cell with $LiBF_4$-PC based Electrolyte by Addition of Small Amount of LiBOB. *J. Power Sources* **2006**, *2*, 629−633.
(9) Niu, C.; Liu, D.; Lochala, J. A.; Anderson, C. S.; Cao, X.; Gross, M. E.; Xu, W.; Zhang, J. G.; Whittingham, M. S.; Xiao, J.; Liu, J. Balancing Interfacial Reactions to Achieve Long Cycle Life in High-Energy Lithium Metal Batteries. *Nat. Energy* **2021**, *6*, 723−732.
(10) Yao, W.; Zhang, Z.; Gao, J.; Li, J.; Xu, J.; Wang, Z.; Yang, Y. Vinyl Ethylene Sulfite as a New Additive in Propylene Carbonate-based Electrolyte for Lithium Ion Batteries. *Energy Environ. Sci.* **2009**, *2*, 1102−1108.
(11) Ping, P.; Xia, X.; Wang, Q. S.; Sun, J. H.; Dahn, J. R. The Effect of Trimethoxyboroxine on Some Positive Electrodes for Li-Ion Batteries. *J. Electrochem. Soc.* **2013**, *160*, A426−A429.
(12) Xu, K. Electrolytes and Interphases in Li-Ion Batteries and Beyond. *Chem. Rev.* **2014**, *114*, 11503−618.
(13) Li, W.; Yao, H.; Yan, K.; Zheng, G.; Liang, Z.; Chiang, Y. M.; Cui, Y. The Synergetic Effect of Lithium Polysulfide and Lithium Nitrate to Prevent Lithium Dendrite Growth. *Nat. Commun.* **2015**, *6*, 7436.
(14) Wu, Y.; Wang, W.; Ming, J.; Li, M.; Xie, L.; He, X.; Wang, J.; Liang, S.; Wu, Y. An Exploration of New Energy Storage System: High Energy Density, High Safety, and Fast Charging Lithium Ion Battery. *Adv. Funct. Mater.* **2019**, *29*, 1805978.
(15) He, Y.; Jiang, L.; Chen, T.; Xu, Y.; Jia, H.; Yi, R.; Xue, D.; Song, M.; Genc, A.; Bouchet-Marquis, C.; Pullan, L.; Tessner, T.; Yoo, J.; Li, X.; Zhang, J. G.; Zhang, S.; Wang, C. Progressive Growth of the Solid-Electrolyte Interphase towards the Si Anode Interior Causes Capacity Fading. *Nat. Nanotechnol.* **2021**, *16*, 1113−1120.
(16) Xia, J.; Dahn, J. R. Improving Sulfolane-based Electrolyte for High Voltage Li-Ion Cells with Electrolyte Additives. *J. Power Sources* **2016**, *324*, 704−711.
(17) Xia, J.; Nelson, K. J.; Lu, Z.; Dahn, J. R. Impact of Electrolyte Solvent and additive Choices on High Voltage Li-ion Pouch Cells. *J. Power Sources* **2016**, *329*, 387−397.
(18) Zheng, J.; Engelhard, M. H.; Mei, D.; Jiao, S.; Polzin, B. J.; Zhang, J. G.; Xu, W. Electrolyte Additive Enabled Fast Charging and Stable Cycling Lithium Metal Batteries. *Nat. Energy* **2017**, *2*, 17012.
(19) Xing, L.; Zheng, X.; Schroeder, M.; Alvarado, J.; von Wald Cresce, A.; Xu, K.; Li, Q.; Li, W. Deciphering the Ethylene Carbonate-Propylene Carbonate Mystery in Li-Ion Batteries. *Acc. Chem. Res.* **2018**, *51*, 282−289.
(20) Wahyudi, W.; Cao, Z.; Kumar, P.; Li, M.; Wu, Y.; Hedhili, M. N.; Anthopoulos, T. D.; Cavallo, L.; Li, L. J.; Ming, J. Phase Inversion Strategy to Flexible Freestanding Electrode: Critical Coupling of Binders and Electrolytes for High Performance Li-S Battery. *Adv. Funct. Mater.* **2018**, *28*, 1802244.
(21) Shadike, Z.; Lee, H.; Borodin, O.; Cao, X.; Fan, X.; Wang, X.; Lin, R.; Bak, S. M.; Ghose, S.; Xu, K.; Wang, C.; Liu, J.; Xiao, J.; Yang, X. Q.; Hu, E. Identification of LiH and Nanocrystalline LiF in the Solid-Electrolyte Interphase of Lithium Metal Anodes. *Nat. Nanotechnol.* **2021**, *16*, 549−554.
(22) Lee, S. H.; Hwang, J. Y.; Ming, J.; Kim, H.; Jung, H. G.; Sun, Y. K. Long-Lasting Solid Electrolyte Interphase for Stable Li-Metal Batteries. *ACS Energy Lett.* **2021**, *6*, 2153−2161.
(23) Ming, J.; Li, M.; Kumar, P.; Lu, A. Y.; Wahyudi, W.; Li, L. J. Redox Species-Based Electrolytes for Advanced Rechargeable Lithium Ion Batteries. *ACS Energy Lett.* **2016**, *1*, 529−534.
(24) Ming, J.; Cao, Z.; Wahyudi, W.; Li, M.; Kumar, P.; Wu, Y.; Hwang, J. Y.; Hedhili, M. N.; Cavallo, L.; Sun, Y. K.; Li, L. J. New Insights on Graphite Anode Stability in Rechargeable Batteries: Li Ion Coordination Structures Prevail over Solid Electrolyte Interphases. *ACS Energy Lett.* **2018**, *3*, 335−340.
(25) Ming, J.; Cao, Z.; Li, Q.; Wahyudi, W.; Wang, W.; Cavallo, L.; Park, K. J.; Sun, Y. K.; Alshareef, H. N. Molecular-Scale Interfacial Model for Predicting Electrode Performance in Rechargeable Batteries. *ACS Energy Lett.* **2019**, *4*, 1584−1593.
(26) Ming, J.; Cao, Z.; Wu, Y.; Wahyudi, W.; Wang, W.; Guo, X.; Cavallo, L.; Hwang, J. Y.; Shamim, A.; Li, L. J.; Sun, Y. K.; Alshareef, H. N. New Insight on the Role of Electrolyte Additives in Rechargeable Lithium Ion Batteries. *ACS Energy Lett.* **2019**, *4*, 2613−2622.
(27) Li, Q.; Cao, Z.; Wahyudi, W.; Liu, G.; Park, G. T.; Cavallo, L.; Anthopoulos, T. D.; Wang, L.; Sun, Y. K.; Alshareef, H. N.; Ming, J. Unraveling the New Role of an Ethylene Carbonate Solvation Shell in Rechargeable Metal Ion Batteries. *ACS Energy Lett.* **2021**, *6*, 69−78.
(28) Liu, G.; Cao, Z.; Zhou, L.; Zhang, J.; Sun, Q.; Hwang, J. Y.; Cavallo, L.; Wang, L.; Sun, Y. K.; Ming, J. Additives Engineered Nonflammable Electrolyte for Safer Potassium Ion Batteries. *Adv. Funct. Mater.* **2020**, *30*, 2001934.
(29) Zhang, J.; Cao, Z.; Zhou, L.; Liu, G.; Park, G.-T.; Cavallo, L.; Wang, L.; Alshareef, H. N.; Sun, Y.-K.; Ming, J. Model-Based Design of Graphite-Compatible Electrolytes in Potassium-Ion Batteries. *ACS Energy Lett.* **2020**, *5*, 2651−2661.
(30) Zhang, J.; Cao, Z.; Zhou, L.; Park, G. T.; Cavallo, L.; Wang, L.; Alshareef, H. N.; Sun, Y. K.; Ming, J. Model-Based Design of Stable Electrolytes for Potassium Ion Batteries. *ACS Energy Lett.* **2020**, *5*, 3124−3131.
(31) Zhou, L.; Cao, Z.; Zhang, J.; Sun, Q.; Wu, Y.; Wahyudi, W.; Hwang, J. Y.; Wang, L.; Cavallo, L.; Sun, Y. K.; Alshareef, H. N.; Ming, J. Engineering Sodium-Ion Solvation Structure to Stabilize Sodium Anodes: Universal Strategy for Fast-Charging and Safer Sodium-Ion Batteries. *Nano Lett.* **2020**, *20*, 3247−3254.
(32) Zou, Y.; Shen, Y.; Wu, Y.; Xue, H.; Guo, Y.; Liu, G.; Wang, L.; Ming, J. A Designed Durable Electrolyte for High-Voltage Lithium-Ion Batteries and Mechanism Analysis. *Chem. - Eur. J.* **2020**, *26*, 7930−7936.
(33) Sun, Q.; Cao, Z.; Zhang, J.; Cheng, H.; Zhang, J.; Li, Q.; Ming, H.; Liu, G.; Ming, J. Metal Catalyst to Construct Carbon Nanotubes Networks on Metal Oxide Microparticles towards Designing High-Performance Electrode for High-Voltage Lithium-Ion Batteries. *Adv. Funct. Mater.* **2021**, *31*, 2009122.
(34) Wahyudi, W.; Ladelta, V.; Tsetseris, L.; Alsabban, M. M.; Guo, X.; Yengel, E.; Faber, H.; Adilbekova, B.; Seitkhan, A.; Emwas, A. H.; Hedhili, M. N.; Li, L. J.; Tung, V.; Hadjichristidis, N.; Anthopoulos, T. D.; Ming, J. Lithium-Ion Desolvation Induced by Nitrate Additives

https://doi.org/10.1021/acsenergylett.1c02425
ACS Energy Lett. 2022, 7, 490−513

Reveals New Insights into High Performance Lithium Batteries. *Adv. Funct. Mater.* **2021**, *31*, 2101593.
(35) Zhou, L.; Cao, Z.; Zhang, J.; Cheng, H.; Liu, G.; Park, G. T.; Cavallo, L.; Wang, L.; Alshareef, H. N.; Sun, Y. K.; Ming, J. Electrolyte-Mediated Stabilization of High-Capacity Micro-Sized Antimony Anodes for Potassium-Ion Batteries. *Adv. Mater.* **2021**, *33*, e2005993.
(36) Zou, Y.; Cao, Z.; Zhang, J.; Wahyudi, W.; Wu, Y.; Liu, G.; Li, Q.; Cheng, H.; Zhang, D.; Park, G. T.; Cavallo, L.; Anthopoulos, T. D.; Wang, L.; Sun, Y. K.; Ming, J. Interfacial Model Deciphering High-Voltage Electrolytes for High Energy Density, High Safety, and Fast-Charging Lithium-Ion Batteries. *Adv. Mater.* **2021**, *33*, e2102964.
(37) Lee, S. H.; Hwang, J. Y.; Ming, J.; Cao, Z.; Nguyen, H. A.; Jung, H. G.; Kim, J.; Sun, Y. K. Toward the Sustainable Lithium Metal Batteries with a New Electrolyte Solvation Chemistry. *Adv. Energy Mater.* **2020**, *10*, 2000567.
(38) Yan, C.; Li, H. R.; Chen, X.; Zhang, X. Q.; Cheng, X. B.; Xu, R.; Huang, J. Q.; Zhang, Q. Regulating the Inner Helmholtz Plane for Stable Solid Electrolyte Interphase on Lithium Metal Anodes. *J. Am. Chem. Soc.* **2019**, *141*, 9422−9429.
(39) Zhang, X. Q.; Chen, X.; Hou, L. P.; Li, B. Q.; Cheng, X. B.; Huang, J. Q.; Zhang, Q. Regulating Anions in the Solvation Sheath of Lithium Ions for Stable Lithium Metal Batteries. *ACS Energy Lett.* **2019**, *4*, 411−416.
(40) Deng, W.; Dai, W.; Zhou, X.; Han, Q.; Fang, W.; Dong, N.; He, B.; Liu, Z. Competitive Solvation-Induced Concurrent Protection on the Anode and Cathode toward a 400 Wh kg^{-1} Lithium Metal Battery. *ACS Energy Lett.* **2021**, *6*, 115−123.
(41) Holoubek, J.; Yu, M.; Yu, S.; Li, M.; Wu, Z.; Xia, D.; Bhaladhare, P.; Gonzalez, M. S.; Pascal, T. A.; Liu, P.; Chen, Z. An All-Fluorinated Ester Electrolyte for Stable High-Voltage Li Metal Batteries Capable of Ultra-Low-Temperature Operation. *ACS Energy Lett.* **2020**, *5*, 1438−1447.
(42) Yang, H.; Chen, X.; Yao, N.; Piao, N.; Wang, Z.; He, K.; Cheng, H. M.; Li, F. Dissolution−Precipitation Dynamics in Ester Electrolyte for High-Stability Lithium Metal Batteries. *ACS Energy Lett.* **2021**, 1413−1421.
(43) Yu, L.; Chen, S.; Lee, H.; Zhang, L.; Engelhard, M. H.; Li, Q.; Jiao, S.; Liu, J.; Xu, W.; Zhang, J.-G. A Localized High-Concentration Electrolyte with Optimized Solvents and Lithium Difluoro(oxalate)-borate Additive for Stable Lithium Metal Batteries. *ACS Energy Lett.* **2018**, *3*, 2059−2067.
(44) Lewis, J. A.; Cortes, F. J. Q.; Boebinger, M. G.; Tippens, J.; Marchese, T. S.; Kondekar, N.; Liu, X.; Chi, M.; McDowell, M. T. Interphase Morphology between a Solid-State Electrolyte and Lithium Controls Cell Failure. *ACS Energy Lett.* **2019**, *4*, 591−599.
(45) Wang, X.; Mai, W.; Guan, X.; Liu, Q.; Tu, W.; Li, W.; Kang, F.; Li, B. Recent Advances of Electroplating Additives Enabling Lithium Metal Anodes to Applicable Battery Techniques. *Energy Environ. Mater.* **2021**, *4*, 284−292.
(46) Fan, J. J.; Dai, P.; Shi, C. G.; Wen, Y.; Luo, C. X.; Yang, J.; Song, C.; Huang, L.; Sun, S. G. Synergistic Dual-Additive Electrolyte for Interphase Modification to Boost Cyclability of Layered Cathode for Sodium Ion Batteries. *Adv. Funct. Mater.* **2021**, *31*, 2010500.
(47) Jiang, R.; Hong, L.; Liu, Y.; Wang, Y.; Patel, S.; Feng, X.; Xiang, H. An Acetamide Additive Stabilizing Ultra-Low Concentration Electrolyte for Long-Cycling and High-Rate Sodium Metal Battery. *Energy Storage Mater.* **2021**, *42*, 370−379.
(48) Dey, A. N.; Sullivan, B. P. The Electrochemical Decomposition of Propylene Carbonate on Graphite. *J. Electrochem. Soc.* **1970**, *117*, 222−224.
(49) Peled, E. The Electrochemical Behavior of Alkali and Alkaline Earth Metals in Nonaqueous Battery Systems-The Solid Electrolyte Interphase Model. Journal of The Electrochemical Society. *J. Electrochem. Soc.* **1979**, *126*, 2047.
(50) Peled, E. Film Forming Reaction at the Lithium/Electrolyte Interface. *J. Power Sources* **1983**, *9*, 253−266.
(51) Fong, R.; von Sacken, U.; Dahn, J. R. Studies of Lithium Intercalation into Carbons Using Nonaqueous Electrochemical Cells. *J. Electrochem. Soc.* **1990**, *137*, 2009−2013.
(52) Goodenough, J. B.; Kim, Y. Challenges for Rechargeable Li Batteries. *Chem. Mater.* **2010**, *22*, 587−603.
(53) Aurbach, D.; Levi, M. D.; Levi, E.; Schechter, A. Failure and Stabilization Mechanisms of Graphite Electrodes. *J. Phys. Chem. B* **1997**, *101*, 2195−2206.
(54) Besenhard, J. O.; Wagner, M. W.; Winter, M.; Jannakoudakis, A. D.; Jannakoudakis, P. D.; Theodoridou, E. Inorganic Film-Forming Electrolyte Additives Improving the Cycling Behaviour of Metallic Lithium Electrodes and the Self-discharge of Carbon-Lithium Electrodes. *J. Power Sources* **1993**, *44*, 413−420.
(55) Wrodnigg, G. H.; Wrodnigg, T. M.; Besenhard, J. O.; Winter, M. Propylene Sulfite as Film-Forming Electrolyte Additive in Lithium Ion Batteries. *Electrochem. Commun.* **1999**, *1*, 148−150.
(56) Wrodnigg, G. H.; Besenhard, J. O.; Winter, M. Ethylene Sulfite as Electrolyte Additive for Lithium-Ion Cells with Graphitic Anodes. *J. Electrochem. Soc.* **1999**, *146*, 470−472.
(57) Peled, E.; Golodnitsky, D.; Ardel, G. Advanced Model for Solid Electrolyte Interphase Electrodes in Liquid and Polymer Electrolytes. *J. Electrochem. Soc.* **1997**, *144*, L208−L210.
(58) Li, T.; Balbuena, P. B. Theoretical Studies of the Reduction of Ethylene Carbonate. *Chem. Phys. Lett.* **2000**, *317*, 421−429.
(59) Wang, Y.; Nakamura, S.; Ue, M.; Balbuena, P. B. Theoretical Studies To Understand Surface Chemistry on Carbon Anodes for Lithium-Ion Batteries: Reduction Mechanisms of Ethylene Carbonate. *J. Am. Chem. Soc.* **2001**, *123*, 11708−11718.
(60) Edström, K.; Gustafsson, T.; Thomas, J. O. The Cathode-Electrolyte Interface in the Li-ion Battery. *Electrochim. Acta* **2004**, *50*, 397−403.
(61) Aurbach, D.; Gamolsky, K.; Markovsky, B.; Gofer, Y.; Schmidt, M.; Heider, U. On the Use of Vinylene Carbonate (VC) as an Additive to Electrolyte Solutions for Li-Ion Batteries. *Electrochim. Acta* **2002**, *47*, 1423−1439.
(62) Hirasawa, K. A.; Sato, T.; Asahina, H.; Yamaguchi, S.; Mori, S. In Situ Electrochemical Atomic Force Microscope Study on Graphite Electrodes. *J. Electrochem. Soc.* **1997**, *144*, L81−L84.
(63) Zhang, Z.; Fouchard, D.; Rea, J. R. Differential Scanning Calorimetry Material Studies: Implications for the Safety of Lithium-Ion Cells. *J. Power Sources* **1998**, *70*, 16−20.
(64) Zhao, L.; Watanabe, I.; Doi, T.; Okada, S.; Yamaki, J. TG-MS Analysis of Solid Electrolyte interphase (SEI) on Graphite Negative-Electrode in Lithium-Ion Batteries. *J. Power Sources* **2006**, *161*, 1275−1280.
(65) Lin, X. M.; Cui, Y.; Xu, Y. H.; Ren, B.; Tian, Z. Q. Surface-Enhanced Raman Spectroscopy: Substrate-Related Issues. *Anal. Bioanal. Chem.* **2009**, *394*, 1729−45.
(66) Wu, M.; Wen, Z.; Liu, Y.; Wang, X.; Huang, L. Electrochemical Behaviors of a Li_3N Modified Li Metal Electrode in Secondary Lithium Batteries. *J. Power Sources* **2011**, *196*, 8091−8097.
(67) Xu, W.; Vegunta, S. S. S.; Flake, J. C. Surface-modified Silicon Nanowire Anodes for Lithium-Ion Batteries. *J. Power Sources* **2011**, *196*, 8583−8589.
(68) Zhang, J.; Wang, R.; Yang, X.; Lu, W.; Wu, X.; Wang, X.; Li, H.; Chen, L. Direct Observation of Inhomogeneous Solid Electrolyte Interphase on MnO Anode with Atomic Force Microscopy and Spectroscopy. *Nano Lett.* **2012**, *12*, 2153−7.
(69) Yang, G.; Ivanov, I. N.; Ruther, R. E.; Sacci, R. L.; Subjakova, V.; Hallinan, D. T.; Nanda, J. Electrolyte Solvation Structure at Solid-Liquid Interface Probed by Nanogap Surface-Enhanced Raman Spectroscopy. *ACS Nano* **2018**, *12*, 10159−10170.
(70) Li, Y.; Li, Y.; Pei, A.; Yan, K.; Sun, Y.; Wu, C. L.; Joubert, L. M.; Chin, R.; Koh, A. L.; Yu, Y.; Perrino, J.; Butz, B.; Chu, S.; Cui, Y. Atomic Structure of Sensitive Battery Materials and Interfaces Revealed by Cryo-Electron Microscopy. *Science* **2017**, *358*, 506−510.
(71) Wang, W.; Cao, Z.; Elia, G. A.; Wu, Y.; Wahyudi, W.; Abou-Hamad, E.; Emwas, A.-H.; Cavallo, L.; Li, L. J.; Ming, J. Recognizing the Mechanism of Sulfurized Polyacrylonitrile Cathode Materials for

https://doi.org/10.1021/acsenergylett.1c02425
ACS Energy Lett. 2022, 7, 490−513

Li-S Batteries and beyond in Al-S Batteries. *ACS Energy Lett.* **2018**, *3*, 2899−2907.
(72) Zhou, L.; Zhang, J.; Wu, Y.; Wang, W.; Ming, H.; Sun, Q.; Wang, L.; Ming, J.; Alshareef, H. N. Understanding Ostwald Ripening and Surface Charging Effects in Solvothermally-Prepared Metal Oxide-Carbon Anodes for High Performance Rechargeable Batteries. *Adv. Energy Mater.* **2019**, *9*, 1902194.
(73) Xue, H.; Wu, Y.; Zou, Y.; Shen, Y.; Liu, G.; Li, Q.; Yin, D.; Wang, L.; Ming, J. Unraveling Metal Oxide Role in Exfoliating Graphite: New Strategy to Construct High-Performance Graphene-Modified SiO_x -Based Anode for Lithium-Ion Batteries. *Adv. Funct. Mater.* **2020**, *30*, 1910657.
(74) Alvarado, J.; Schroeder, M. A.; Pollard, T. P.; Wang, X.; Lee, J. Z.; Zhang, M.; Wynn, T.; Ding, M.; Borodin, O.; Meng, Y. S.; Xu, K. Bisalt Ether Electrolytes: A Pathway towards Lithium Metal Batteries with Ni-rich Cathodes. *Energy Environ. Sci.* **2019**, *12*, 780−794.
(75) Abe, T.; Fukuda, H.; Iriyama, Y.; Ogumi, Z. Solvated Li-Ion Transfer at Interface Between Graphite and Electrolyte. *J. Electrochem. Soc.* **2004**, *151*, A1120.
(76) Jiang, L. L.; Yan, C.; Yao, Y. X.; Cai, W.; Huang, J. Q.; Zhang, Q. Inhibiting Solvent Cointercalation in a Graphite Anode by a Localized High-Concentration Electrolyte in Fast-Charging Batteries. *Angew. Chem., Int. Ed.* **2021**, *60*, 3402−3406.
(77) Yao, Y. X.; Chen, X.; Yan, C.; Zhang, X. Q.; Cai, W. L.; Huang, J. Q.; Zhang, Q. Regulating Interfacial Chemistry in Lithium-Ion Batteries by a Weakly Solvating Electrolyte. *Angew. Chem., Int. Ed.* **2021**, *60*, 4090−4097.
(78) Liu, X.; Shen, X.; Li, H.; Li, P.; Luo, L.; Fan, H.; Feng, X.; Chen, W.; Ai, X.; Yang, H.; Cao, Y. Ethylene Carbonate-Free Propylene Carbonate-Based Electrolytes with Excellent Electrochemical Compatibility for Li-Ion Batteries through Engineering Electrolyte Solvation Structure. *Adv. Energy Mater.* **2021**, *11*, 2003905.
(79) Yamada, Y.; Yaegashi, M.; Abe, T.; Yamada, A. A Superconcentrated Ether Electrolyte for Fast-Charging Li-Ion Batteries. *ChemComm* **2013**, *49*, 11194−6.
(80) Adams, B. D.; Carino, E. V.; Connell, J. G.; Han, K. S.; Cao, R.; Chen, J.; Zheng, J.; Li, Q.; Mueller, K. T.; Henderson, W. A.; Zhang, J. G. Long Term Stability of Li-S Batteries using High Concentration Lithium Nitrate Electrolytes. *Nano Energy* **2017**, *40*, 607−617.
(81) Alvarado, J.; Schroeder, M. A.; Zhang, M.; Borodin, O.; Gobrogge, E.; Olguin, M.; Ding, M. S.; Gobet, M.; Greenbaum, S.; Meng, Y. S.; Xu, K. A Carbonate-Free, Sulfone-Based Electrolyte for High-Voltage Li-Ion Batteries. *Mater. Today* **2018**, *21*, 341−353.
(82) Ren, X.; Chen, S.; Lee, H.; Mei, D.; Engelhard, M. H.; Burton, S. D.; Zhao, W.; Zheng, J.; Li, Q.; Ding, M. S.; Schroeder, M.; Alvarado, J.; Xu, K.; Meng, Y. S.; Liu, J.; Zhang, J.-G.; Xu, W. Localized High-Concentration Sulfone Electrolytes for High-Efficiency Lithium-Metal Batteries. *Chem.* **2018**, *4*, 1877−1892.
(83) Fu, J.; Ji, X.; Chen, J.; Chen, L.; Fan, X.; Mu, D.; Wang, C. Lithium Nitrate Regulated Sulfone Electrolytes for Lithium Metal Batteries. *Angew. Chem., Int. Ed.* **2020**, *59*, 22194−22201.
(84) Wang, L.; Menakath, A.; Han, F.; Wang, Y.; Zavalij, P. Y.; Gaskell, K. J.; Borodin, O.; Iuga, D.; Brown, S. P.; Wang, C.; Xu, K.; Eichhorn, B. W. Identifying the components of the solid-electrolyte interphase in Li-ion batteries. *Nat. Chem.* **2019**, *11*, 789−796.
(85) Yamada, Y.; Furukawa, K.; Sodeyama, K.; Kikuchi, K.; Yaegashi, M.; Tateyama, Y.; Yamada, A. Unusual Stability of Acetonitrile-Based Superconcentrated Electrolytes for Fast-Charging Lithium-Ion Batteries. *J. Am. Chem. Soc.* **2014**, *136*, 5039−46.
(86) Peng, Z.; Cao, X.; Gao, P.; Jia, H.; Ren, X.; Roy, S.; Li, Z.; Zhu, Y.; Xie, W.; Liu, D.; Li, Q.; Wang, D.; Xu, W.; Zhang, J. G. High-Power Lithium Metal Batteries Enabled by High-Concentration Acetonitrile-Based Electrolytes with Vinylene Carbonate Additive. *Adv. Funct. Mater.* **2020**, *30*, 2001285.
(87) Jia, H.; Xu, Y.; Zhang, X.; Burton, S. D.; Gao, P.; Matthews, B. E.; Engelhard, M. H.; Han, K. S.; Zhong, L.; Wang, C.; Xu, W. Advanced Low-Flammable Electrolytes for Stable Operation of High-Voltage Lithium-Ion Batteries. *Angew. Chem., Int. Ed.* **2021**, *60*, 12999−13006.
(88) Ren, X.; Zou, L.; Cao, X.; Engelhard, M. H.; Liu, W.; Burton, S. D.; Lee, H.; Niu, C.; Matthews, B. E.; Zhu, Z.; Wang, C.; Arey, B. W.; Xiao, J.; Liu, J.; Zhang, J.-G.; Xu, W. Enabling High-Voltage Lithium-Metal Batteries under Practical Conditions. *Joule* **2019**, *3*, 1662−1676.
(89) Chen, S.; Zheng, J.; Mei, D.; Han, K. S.; Engelhard, M. H.; Zhao, W.; Xu, W.; Liu, J.; Zhang, J. G. High-Voltage Lithium-Metal Batteries Enabled by Localized High-Concentration Electrolytes. *Adv. Mater.* **2018**, *30*, e1706102.
(90) Cao, X.; Xu, Y.; Zhang, L.; Engelhard, M. H.; Zhong, L.; Ren, X.; Jia, H.; Liu, B.; Niu, C.; Matthews, B. E.; Wu, H.; Arey, B. W.; Wang, C.; Zhang, J. G.; Xu, W. Nonflammable Electrolytes for Lithium Ion Batteries Enabled by Ultraconformal Passivation Interphases. *ACS Energy Lett.* **2019**, *4*, 2529−2534.
(91) Zhang, S.; Yang, G.; Liu, Z.; Li, X.; Wang, X.; Chen, R.; Wu, F.; Wang, Z.; Chen, L. Competitive Solvation Enhanced Stability of Lithium Metal Anode in Dual-Salt Electrolyte. *Nano Lett.* **2021**, *21*, 3310−3317.
(92) Fan, X.; Chen, L.; Ji, X.; Deng, T.; Hou, S.; Chen, J.; Zheng, J.; Wang, F.; Jiang, J.; Xu, K.; Wang, C. Highly Fluorinated Interphases Enable High-Voltage Li-Metal Batteries. *Chem.* **2018**, *4*, 174−185.
(93) Qian, J.; Henderson, W. A.; Xu, W.; Bhattacharya, P.; Engelhard, M.; Borodin, O.; Zhang, J. G. High Rate and Stable Cycling of Lithium Metal Anode. *Nat. Commun.* **2015**, *6*, 6362.
(94) Qiu, F.; Li, X.; Deng, H.; Wang, D.; Mu, X.; He, P.; Zhou, H. A Concentrated Ternary-Salts Electrolyte for High Reversible Li Metal Battery with Slight Excess Li. *Adv. Energy Mater.* **2019**, *9*, 1803372.
(95) Chen, S.; Zheng, J.; Yu, L.; Ren, X.; Engelhard, M. H.; Niu, C.; Lee, H.; Xu, W.; Xiao, J.; Liu, J.; Zhang, J.-G. High-Efficiency Lithium Metal Batteries with Fire-Retardant Electrolytes. *Joule* **2018**, *2*, 1548−1558.
(96) Born, M. Volumes and Heats of Hydration of Ions. *Zeitschrift für Physik* **1920**, *1*, 45−48.
(97) Onsager, L. Electric Moments of Molecules in Liquids. *J. Am. Chem. Soc.* **1936**, *58*, 1486−1493.
(98) Frank, H. S. Local Dielectric Constant and Solute Activity. A Hydration-Association Model for Strong Electrolytes. *J. Am. Chem. Soc.* **1941**, *63*, 1789−1799.
(99) Frank, H. S.; Evans, M. W. Free Volume and Entropy in Condensed Systems III. Entropy in Binary Liquid Mixtures; Partial Molal Entropy in Dilute Solutions; Structure and Thermodynamics in Aqueous Electrolytes. *J. Chem. Phys.* **1945**, *13*, 507−532.
(100) Stokes, R. H.; Robinson, R. A. Ionic Hydration and Activity in Electrolyte Solutions. *J. Am. Chem. Soc.* **1948**, *70*, 1870−1878.
(101) Cox, B. G.; Parker, A. J.; Waghorne, W. E. Coordination and Ionic Solvation. *J. Phys. Chem.* **1974**, *78*, 1731.
(102) Ghosh, J. C. XXXVIII.-The Abnormality of Strong Electrolytes. Part I. Electrical Conductivity of Aqueous Salt Solutions. *J. Chem. Soc. Trans.* **1918**, *113*, 449−458.
(103) Pitzer, K. S. Thermodynamics of Electrolytes. I. Theoretical Basis and General Equations. *J. Phys. Chem.* **1973**, *77*, 268−277.
(104) Pitzer, K. S.; Mayorga, G. Thermodynamics of Electrolytes. II. Activity and Osmotic Coefficients for Strong Electrolytes with One or Both Ions Univalent. *J. Phys. Chem.* **1973**, *77*, 2300−2308.
(105) Bryantsev, V. S.; Diallo, M. S.; Goddard, W. A., III Calculation of Solvation Free Energies of Charged Solutes Using Mixed Cluster/Continuum Models. *J. Phys. Chem. B* **2008**, *112*, 9709−9719.
(106) Kumar, N.; Seminario, J. M. Lithium-Ion Model Behavior in an Ethylene Carbonate Electrolyte Using Molecular Dynamics. *J. Phys. Chem. C* **2016**, *120*, 16322−16332.
(107) Sun, Y.; Yang, T.; Ji, H.; Zhou, J.; Wang, Z.; Qian, T.; Yan, C. Boosting the Optimization of Lithium Metal Batteries by Molecular Dynamics Simulations: A Perspective. *Adv. Energy Mater.* **2020**, *10*, 2002373.
(108) Marenich, A. V.; Ho, J.; Coote, M. L.; Cramer, C. J.; Truhlar, D. G. Computational Electrochemistry: Prediction of Liquid-Phase Reduction Potentials. *Phys. Chem. Chem. Phys.* **2014**, *16*, 15068−15106.

(109) Bogle, X.; Vazquez, R.; Greenbaum, S.; Cresce, A.; Xu, K. Understanding Li^+-Solvent Interaction in Nonaqueous Carbonate Electrolytes with ^{17}O NMR. *J. Phys. Chem. Lett.* **2013**, *4*, 1664−1668.
(110) Fujii, K.; Hamano, H.; Doi, H.; Song, X.; Tsuzuki, S.; Hayamizu, K.; Seki, S.; Kameda, Y.; Dokko, K.; Watanabe, M.; Umebayashi, Y. Unusual Li^+ Ion Solvation Structure in Bis-(fluorosulfonyl)amide Based Ionic Liquid. *J. Phys. Chem. C* **2013**, *117*, 19314−19324.
(111) Mandai, T.; Yoshida, K.; Ueno, K.; Dokko, K.; Watanabe, M. Criteria for solvate ionic liquids. *Phys. Chem. Chem. Phys.* **2014**, *16*, 8761−8772.
(112) Moon, H.; Tatara, R.; Mandai, T.; Ueno, K.; Yoshida, K.; Tachikawa, N.; Yasuda, T.; Dokko, K.; Watanabe, M. Mechanism of Li Ion Desolvation at the Interface of Graphite Electrode and Glyme-Li Salt Solvate Ionic Liquids. *J. Phys. Chem. C* **2014**, *118*, 20246−20256.
(113) Zhang, C.; Ueno, K.; Yamazaki, A.; Yoshida, K.; Moon, H.; Mandai, T.; Umebayashi, Y.; Dokko, K.; Watanabe, M. Chelate effects in glyme/lithium bis(trifluoromethanesulfonyl)amide solvate ionic liquids. I. Stability of solvate cations and correlation with electrolyte properties. *J. Phys. Chem. B* **2014**, *118*, 5144−53.
(114) Ueno, K.; Murai, J.; Ikeda, K.; Tsuzuki, S.; Tsuchiya, M.; Tatara, R.; Mandai, T.; Umebayashi, Y.; Dokko, K.; Watanabe, M. Li+ Solvation and Ionic Transport in Lithium Solvate Ionic Liquids Diluted by Molecular Solvents. *J. Phys. Chem. C* **2016**, *120*, 15792−15802.
(115) Yamada, Y.; Takazawa, Y.; Miyazaki, K.; Abe, T. Electrochemical Lithium Intercalation into Graphite in Dimethyl Sulfoxide-Based Electrolytes: Effect of Solvation Structure of Lithium Ion. *J. Phys. Chem. C* **2010**, *114*, 11680−11685.
(116) Yamada, Y.; Koyama, Y.; Abe, T.; Ogumi, Z. Correlation between Charge−Discharge Behavior of Graphite and Solvation Structure of the Lithium Ion in Propylene Carbonate-Containing Electrolytes. *J. Phys. Chem. C* **2009**, *113*, 8948−8953.
(117) Ren, X.; Gao, P.; Zou, L.; Jiao, S.; Cao, X.; Zhang, X.; Jia, H.; Engelhard, M. H.; Matthews, B. E.; Wu, H.; Lee, H.; Niu, C.; Wang, C.; Arey, B. W.; Xiao, J.; Liu, J.; Zhang, J. G.; Xu, W. Role of Inner Solvation Sheath within Salt-Solvent Complexes in tailoring Electrode/Electrolyte Interphases for Lithium Metal Batteries. *Proc. Natl. Acad. Sci. U.S.A.* **2020**, *117*, 28603−28613.
(118) Li, Y.; Yang, Y.; Lu, Y.; Zhou, Q.; Qi, X.; Meng, Q.; Rong, X.; Chen, L.; Hu, Y.-S. Ultralow-Concentration Electrolyte for Na-Ion Batteries. *ACS Energy Lett.* **2020**, *5*, 1156−1158.
(119) Abe, T.; Kawabata, N.; Mizutani, Y.; Inaba, M.; Ogumi, Z. Correlation Between Cointercalation of Solvents and Electrochemical Intercalation of Lithium into Graphite in Propylene Carbonate Solution. *J. Electrochem. Soc.* **2003**, *150*, A257.
(120) Li, M.; Wan, Y.; Huang, J. K.; Assen, A. H.; Hsiung, C. E.; Jiang, H.; Han, Y.; Eddaoudi, M.; Lai, Z.; Ming, J.; Li, L. J. Metal-Organic Framework-Based Separators for Enhancing Li-S Battery Stability: Mechanism of Mitigating Polysulfide Diffusion. *ACS Energy Lett.* **2017**, *2*, 2362−2367.
(121) Wang, A.; Kadam, S.; Li, H.; Shi, S.; Qi, Y. Review on Modeling of the Anode Solid Electrolyte Interphase (SEI) for Lithium-Ion Batteries. *NPJ. Comput. Mater.* **2018**, *4*, 15.
(122) Yang, G.; Frisco, S.; Tao, R.; Philip, N.; Bennett, T. H.; Stetson, C.; Zhang, J.-G.; Han, S.-D.; Teeter, G.; Harvey, S. P.; Zhang, Y.; Veith, G. M.; Nanda, J. Robust Solid/Electrolyte Interphase (SEI) Formation on Si Anodes Using Glyme-Based Electrolytes. *ACS Energy Lett.* **2021**, *6*, 1684−1693.
(123) Helmholtz, H. Studien über Electrische Grenzschichten. *Annalen Der Physik Und Chemie* **1879**, *243*, 337−382.
(124) Gouy, M. Sur la constitution de la charge électrique à la surface d'un électrolyte. *Journal de Physique Théorique et Appliquée* **1910**, *9*, 457−468.
(125) Stern, H. O. Zur Theorie der Elektrolytischen Doppelschicht. *Z. Elektrochem. Angew. Phys. Chem.* **1924**, *30*, 508−516.
(126) Bockris, J. O.; Devanathan, M. A. V.; Müller, K. On the Structure of Charged Interfaces. *Proc. R. Soc. London A* **1963**, *274*, 55−79.
(127) Gongadze, E.; Iglic, A. Decrease of Permittivity of an Electrolyte Solution Near a Charged Surface due to Saturation and Excluded Volume Effects. *Bioelectrochemistry* **2012**, *87*, 199−203.
(128) Gongadze, E.; Velikonja, A.; Perutkova, Š.; Kramar, P.; Maček-Lebar, A.; Kralj-Iglič, V.; Iglič, A. Ions and Water Molecules in an Electrolyte Solution in Contact with Charged and Dipolar Surfaces. *Electrochim. Acta* **2014**, *126*, 42−60.
(129) Yoshida, K.; Nakamura, M.; Kazue, Y.; Tachikawa, N.; Tsuzuki, S.; Seki, S.; Dokko, K.; Watanabe, M. Oxidative-Stability Enhancement and Charge Transport Mechanism in Glyme-Lithium Salt Equimolar Complexes. *J. Am. Chem. Soc.* **2011**, *133*, 13121−9.
(130) Jaumaux, P.; Wu, J.; Shanmukaraj, D.; Wang, Y.; Zhou, D.; Sun, B.; Kang, F.; Li, B.; Armand, M.; Wang, G. Non-Flammable Liquid and Quasi-Solid Electrolytes toward Highly-Safe Alkali Metal-Based Batteries. *Adv. Funct. Mater.* **2021**, *31*, 2008644.
(131) Hu, J.; Ren, W.; Chen, X.; Li, Y.; Huang, W.; Yang, K.; Yang, L.; Lin, Y.; Zheng, J.; Pan, F. The Role of Anions on the Helmholtz Plane for the Solid-Liquid Interface in Aqueous Rechargeable Lithium Batteries. *Nano Energy* **2020**, *74*, 104864.
(132) Fan, L.; Ma, R.; Zhang, Q.; Jia, X.; Lu, B. Graphite Anode for a Potassium-Ion Battery with Unprecedented Performance. *Angew. Chem., Int. Ed.* **2019**, *58*, 10500−10505.
(133) Niu, X.; Li, L.; Qiu, J.; Yang, J.; Huang, J.; Wu, Z.; Zou, J.; Jiang, C.; Gao, J.; Wang, L. Salt-Concentrated Electrolytes for Graphite Anode in Potassium Ion Battery. *Solid State Ionics* **2019**, *341*, 115050.
(134) Zeng, G.; Xiong, S.; Qian, Y.; Ci, L.; Feng, J. Non-Flammable Phosphate Electrolyte with High Salt-to-Solvent Ratios for Safe Potassium-Ion Battery. *J. Electrochem. Soc.* **2019**, *166*, A1217−A1222.
(135) Liu, S.; Mao, J.; Zhang, L.; Pang, W. K.; Du, A.; Guo, Z. Manipulating the Solvation Structure of Nonflammable Electrolyte and Interface to Enable Unprecedented Stability of Graphite Anodes beyond 2 Years for Safe Potassium-Ion Batteries. *Adv. Mater.* **2021**, *33*, e2006313.
(136) Yang, H.; Chen, C. Y.; Hwang, J.; Kubota, K.; Matsumoto, K.; Hagiwara, R. Potassium Difluorophosphate as an Electrolyte Additive for Potassium-Ion Batteries. *ACS Appl. Mater. Interfaces* **2020**, *12*, 36168−36176.
(137) Gu, M.; Fan, L.; Zhou, J.; Rao, A. M.; Lu, B. Regulating Solvent Molecule Coordination with KPF6 for Superstable Graphite Potassium Anodes. *ACS Nano* **2021**, *15*, 9167−9175.
(138) Wang, L.; Huang, Y.; Jia, D. Triethyl Orthoformate as a New Film-Forming Electrolytes Solvent for Lithium-Ion Batteries with Graphite Anodes. *Electrochim. Acta* **2006**, *51*, 4950−4955.
(139) Xu, M. Q.; Li, W. S.; Zuo, X. X.; Liu, J. S.; Xu, X. Performance Improvement of Lithium Ion Battery using PC as a Solvent Component and BS as an SEI Forming Additive. *J. Power Sources* **2007**, *174*, 705−710.
(140) Wang, B.; Qu, Q. T.; Yang, L. C.; Xia, Q.; Wu, Y. P.; Zhou, D. L.; Gu, X. J.; van Ree, T. 2-Phenylimidazole as an Additive to Prevent the Cointercalation of Propylene Carbonate in Organic Electrolyte for Lithium-Ion Batteries. *J. Power Sources* **2009**, *189*, 757−760.
(141) Li, B.; Xu, M.; Li, T.; Li, W.; Hu, S. Prop-1-ene-1,3-sultone as SEI Formation Additive in Propylene Carbonate-Based Electrolyte for Lithium Ion Batteries. *Electrochem. Commun.* **2012**, *17*, 92−95.
(142) Mai, S.; Xu, M.; Wang, Y.; Liao, X.; Lin, H.; Li, W. Methylene Methanedisulfonate (MMDS) as a Novel SEI Forming Additive on Anode for Lithium Ion Batteries. *Int. J. Electrochem. Sci.* **2014**, *9*, 6294−6304.
(143) Qin, L.; Xiao, N.; Zheng, J.; Lei, Y.; Zhai, D.; Wu, Y. Localized High-Concentration Electrolytes Boost Potassium Storage in High-Loading Graphite. *Adv. Energy Mater.* **2019**, *9*, 1902618.
(144) Flores, E.; Åvall, G.; Jeschke, S.; Johansson, P. Solvation Structure in Dilute to Highly Concentrated Electrolytes for Lithium-Ion and Sodium-Ion Batteries. *Electrochim. Acta* **2017**, *233*, 134−141.

https://doi.org/10.1021/acsenergylett.1c02425
ACS Energy Lett. 2022, 7, 490−513

(145) Takada, K.; Yamada, Y.; Watanabe, E.; Wang, J.; Sodeyama, K.; Tateyama, Y.; Hirata, K.; Kawase, T.; Yamada, A. Unusual Passivation Ability of Superconcentrated Electrolytes toward Hard Carbon Negative Electrodes in Sodium-Ion Batteries. *ACS Appl. Energy Mater.* **2017**, *9*, 33802−33809.
(146) Geng, C.; Buchholz, D.; Kim, G. T.; Carvalho, D. V.; Zhang, H.; Chagas, L. G.; Passerini, S. Influence of Salt Concentration on the Properties of Sodium-Based Electrolytes. *Small Methods* **2019**, *3*, 1800208.
(147) Ao, H.; Chen, C.; Hou, Z.; Cai, W.; Liu, M.; Jin, Y.; Zhang, X.; Zhu, Y.; Qian, Y. Electrolyte Solvation Structure Manipulation Enables Safe and Stable Aqueous Sodium Ion Batteries. *J. Mater. Chem. A* **2020**, *8*, 14190−14197.
(148) Hou, Z.; Dong, M.; Xiong, Y.; Zhang, X.; Zhu, Y.; Qian, Y. Formation of Solid−Electrolyte Interfaces in Aqueous Electrolytes by Altering Cation-Solvation Shell Structure. *Adv. Energy Mater.* **2020**, *10*, 1903665.
(149) Bai, P.; Han, X.; He, Y.; Xiong, P.; Zhao, Y.; Sun, J.; Xu, Y. Solid Electrolyte Interphase Manipulation towards Highly Stable Hard Carbon Anodes for sodium Ion Batteries. *Energy Stor. Mater.* **2020**, *25*, 324−333.
(150) Shi, J.; Ding, L.; Wan, Y.; Mi, L.; Chen, L.; Yang, D.; Hu, Y.; Chen, W. Achieving Long-Cycling Sodium-Ion Full Cells in Ether-Based Electrolyte with Vinylene Carbonate Additive. *J. Energy Chem.* **2021**, *57*, 650−655.
(151) Sun, T.; Feng, X.; Sun, Q.; Yu, Y.; Yuan, G.; Xiong, Q.; Liu, D.; Zhang, X.; Zhang, Y. Solvation Effect on the Improved Sodium Storage Performance of N-heteropentacenequinone. *Angew. Chem., Int. Ed.* **2021**, *133*, 27010−27016.
(152) Liang, H. J.; Gu, Z. Y.; Zhao, X. X.; Guo, J. Z.; Yang, J. L.; Li, W. H.; Li, B.; Liu, Z. M.; Li, W. L.; Wu, X. L. Universal Ether-Based Electrolyte Chemistry towards High-Voltage and Long-Life Na-Ion Full Batteries. *Angew. Chem., Int. Ed.* **2021**, *60*, 26837−26846.
(153) Yang, Z.; Chou, S.; He, J.; Lai, W. H.; Peng, J.; Liu, X. H.; He, X. X.; Guo, X. F.; Li, L.; Qiao, Y.; Ma, J. M.; Wu, M. Fire-Retardant, Stable-Cycling and High-Safety Sodium Ion Battery. *Angew. Chem., Int. Ed.* **2021**, *60*, 27086−27094.
(154) Zhou, L.; Cao, Z.; Wahyudi, W.; Zhang, J.; Hwang, J.-Y.; Cheng, Y.; Wang, L.; Cavallo, L.; Anthopoulos, T.; Sun, Y. K.; Alshareef, H. N.; Ming, J. Electrolyte Engineering Enables High Stability and Capacity Alloying Anodes for Sodium and Potassium Ion Batteries. *ACS Energy Lett.* **2020**, *5*, 766−776.
(155) Xiong, B. Q.; Zhou, X.; Xu, G. L.; Liu, Y.; Zhu, L.; Hu, Y.; Shen, S. Y.; Hong, Y. H.; Wan, S. C.; Liu, X. C.; Liu, X.; Chen, S.; Huang, L.; Sun, S. G.; Amine, K.; Ke, F. S. Boosting Superior Lithium Storage Performance of Alloy-Based Anode Materials via Ultra-conformal Sb Coating-Derived Favorable Solid-Electrolyte Interphase. *Adv. Energy Mater.* **2020**, *10*, 1903186.
(156) Wang, H.; Fu, J.; Wang, C.; Wang, J.; Yang, A.; Li, C.; Sun, Q.; Cui, Y.; Li, H. A binder-free high silicon content flexible anode for Li-ion batteries. *Energy Environ. Sci.* **2020**, *13*, 848−858.
(157) Zhu, Z.; Wang, S.; Du, J.; Jin, Q.; Zhang, T.; Cheng, F.; Chen, J. Ultrasmall Sn Nanoparticles Embedded in Nitrogen-Doped Porous Carbon as High-Performance Anode for Lithium-Ion Batteries. *Nano Lett.* **2014**, *14*, 153−7.
(158) Liu, Z.; Yu, X.-Y.; Lou, X. W.; Paik, U. Sb@C Coaxial Nanotubes as A Superior Long-Life and High-Rate Anode for Sodium Ion Batteries. *Energy Environ. Sci.* **2016**, *9*, 2314−2318.
(159) Chan, C. K.; Peng, H.; Liu, G.; McIlwrath, K.; Zhang, X. F.; Huggins, R. A.; Cui, Y. High-Performance Lithium Battery Anodes Using Silicon Nanowires. *Nat. Nanotechnol.* **2008**, *3*, 31−5.
(160) Wang, S.; Yi, Z.; Wang, X.; Sun, Q.; Cheng, Y.; Wang, L. A Rational Design to Buffer Volume Expansion of CoSn Intermetallic in Lithium and Sodium Storage: Multicore-Shell versus Monocore-Shell. *Energy Stor. Mater.* **2019**, *23*, 629−635.
(161) Du, X.; Gao, Y.; Zhang, B. Building Elastic Solid Electrolyte Interphases for Stabilizing Microsized Antimony Anodes in Potassium Ion Batteries. *Adv. Funct. Mater.* **2021**, *31*, 2102562.
(162) Jia, H.; Zou, L.; Gao, P.; Cao, X.; Zhao, W.; He, Y.; Engelhard, M. H.; Burton, S. D.; Wang, H.; Ren, X.; Li, Q.; Yi, R.; Zhang, X.; Wang, C.; Xu, Z.; Li, X.; Zhang, J. G.; Xu, W. High-Performance Silicon Anodes Enabled By Nonflammable Localized High-Concentration Electrolytes. *Adv. Energy Mater.* **2019**, *9*, 1900784.
(163) Cao, Z.; Zheng, X.; Qu, Q.; Huang, Y.; Zheng, H. Electrolyte Design Enabling a High-Safety and High-Performance Si Anode with a Tailored Electrode-Electrolyte Interphase. *Adv. Mater.* **2021**, *33*, e2103178.
(164) Chen, J.; Fan, X.; Li, Q.; Yang, H.; Khoshi, M. R.; Xu, Y.; Hwang, S.; Chen, L.; Ji, X.; Yang, C.; He, H.; Wang, C.; Garfunkel, E.; Su, D.; Borodin, O.; Wang, C. Electrolyte design for LiF-rich solid-electrolyte interfaces to enable high-performance microsized alloy anodes for batteries. *Nat. Energy* **2020**, *5*, 386−397.
(165) Chae, S.; Kwak, W. J.; Han, K. S.; Li, S.; Engelhard, M. H.; Hu, J.; Wang, C.; Li, X.; Zhang, J. G. Rational Design of Electrolytes for Long-Term Cycling of Si Anodes over a Wide Temperature Range. *ACS Energy Lett.* **2021**, *6*, 387−394.
(166) Wang, H.; Yu, D.; Wang, X.; Niu, Z.; Chen, M.; Cheng, L.; Zhou, W.; Guo, L. Electrolyte Chemistry Enables Simultaneous Stabilization of Potassium Metal and Alloying Anode for Potassium-Ion Batteries. *Angew. Chem., Int. Ed.* **2019**, *58*, 16451−16455.
(167) Li, Q.; Cao, Z.; Liu, G.; Cheng, H.; Wu, Y.; Ming, H.; Park, G. T.; Yin, D.; Wang, L.; Cavallo, L.; Sun, Y. K.; Ming, J. Electrolyte Chemistry in 3D Metal Oxide Nanorod Arrays Deciphers Lithium Dendrite-Free Plating/Stripping Behaviors for High-Performance Lithium Batteries. *J. Phys. Chem. Lett.* **2021**, *12*, 4857−4866.
(168) Petibon, R.; Xia, J.; Ma, L.; Bauer, M. K. G.; Nelson, K. J.; Dahn, J. R. Electrolyte System for High Voltage Li-Ion Cells. *J. Electrochem. Soc.* **2016**, *163*, A2571−A2578.
(169) Logan, E. R.; Tonita, E. M.; Gering, K. L.; Ma, L.; Bauer, M. K. G.; Li, J.; Beaulieu, L. Y.; Dahn, J. R. A Study of the Transport Properties of Ethylene Carbonate-Free Li Electrolytes. *J. Electrochem. Soc.* **2018**, *165*, A705−A716.
(170) Klein, S.; van Wickeren, S.; Röser, S.; Bärmann, P.; Borzutzki, K.; Heidrich, B.; Börner, M.; Winter, M.; Placke, T.; Kasnatscheew, J. Understanding the Outstanding High-Voltage Performance of NCM523||Graphite Lithium Ion Cells after Elimination of Ethylene Carbonate Solvent from Conventional Electrolyte. *Adv. Energy Mater.* **2021**, *11*, 2003738.
(171) Qian, J.; Adams, B. D.; Zheng, J.; Xu, W.; Henderson, W. A.; Wang, J.; Bowden, M. E.; Xu, S.; Hu, J.; Zhang, J.-G. Anode-Free Rechargeable Lithium Metal Batteries. *Adv. Funct. Mater.* **2016**, *26*, 7094−7102.
(172) Weber, R.; Genovese, M.; Louli, A. J.; Hames, S.; Martin, C.; Hill, I. G.; Dahn, J. R. Long Cycle Life and Dendrite-Free Lithium Morphology in Anode-Free Lithium Pouch Cells Enabled by a Dual-Salt Liquid Electrolyte. *Nat. Energy* **2019**, *4*, 683−689.
(173) Eldesoky, A.; Louli, A. J.; Benson, A.; Dahn, J. R. Cycling Performance of NMC811 Anode-Free Pouch Cells with 65 Different Electrolyte Formulations. *J. Electrochem. Soc.* **2021**, *168*, 120508.
(174) Xiao, N.; McCulloch, W. D.; Wu, Y. Reversible Dendrite-Free Potassium Plating and Stripping Electrochemistry for Potassium Secondary Batteries. *J. Am. Chem. Soc.* **2017**, *139*, 9475−9478.
(175) Zhang, X. Q.; Chen, X.; Cheng, X. B.; Li, B. Q.; Shen, X.; Yan, C.; Huang, J. Q.; Zhang, Q. Highly Stable Lithium Metal Batteries Enabled by Regulating the Solvation of Lithium Ions in Nonaqueous Electrolytes. *Angew. Chem., Int. Ed.* **2018**, *57*, 5301−5305.
(176) Zheng, J.; Chen, S.; Zhao, W.; Song, J.; Engelhard, M. H.; Zhang, J.-G. Extremely Stable Sodium Metal Batteries Enabled by Localized High-Concentration Electrolytes. *ACS Energy Lett.* **2018**, *3*, 315−321.
(177) Yu, Z.; Wang, H.; Kong, X.; Huang, W.; Tsao, Y.; Mackanic, D. G.; Wang, K.; Wang, X.; Huang, W.; Choudhury, S.; Zheng, Y.; Amanchukwu, C. V.; Hung, S. T.; Ma, Y.; Lomeli, E. G.; Qin, J.; Cui, Y.; Bao, Z. Molecular Design for Electrolyte Solvents enabling Energy-Dense and Long-Cycling Lithium Metal Batteries. *Nat. Energy* **2020**, *5*, 526−533.

https://doi.org/10.1021/acsenergylett.1c02425
ACS Energy Lett. 2022, 7, 490−513

(178) Liu, X.; Zheng, X.; Dai, Y.; Wu, W.; Huang, Y.; Fu, H.; Huang, Y.; Luo, W. Fluoride-Rich Solid-Electrolyte-Interface Enabling Stable Sodium Metal Batteries in High-Safe Electrolytes. *Adv. Funct. Mater.* **2021**, *31*, 2103522.
(179) Xiao, D.; Li, Q.; Luo, D.; Li, G.; Liu, H.; Shui, L.; Gourley, S.; Zhou, G.; Wang, X.; Chen, Z. Regulating the Li^+ -Solvation Structure of Ester Electrolyte for High-Energy-Density Lithium Metal Batteries. *Small* **2020**, *16*, e2004688.
(180) Wang, Y.; Jiang, R.; Liu, Y.; Zheng, H.; Fang, W.; Liang, X.; Sun, Y.; Zhou, R.; Xiang, H. Enhanced Sodium Metal/Electrolyte Interface by a Localized High-Concentration Electrolyte for Sodium Metal Batteries: First-Principles Calculations and Experimental Studies. *ACS Appl. Energy Mater.* **2021**, *4*, 7376−7384.
(181) Holoubek, J.; Liu, H.; Wu, Z.; Yin, Y.; Xing, X.; Cai, G.; Yu, S.; Zhou, H.; Pascal, T. A.; Chen, Z.; Liu, P. Tailoring Electrolyte Solvation for Li Metal Batteries Cycled at Ultra-Low Temperature. *Nat. Energy* **2021**, *6*, 303−313.
(182) Li, Q.; Liu, G.; Cheng, H.; Sun, Q.; Zhang, J.; Ming, J. Low-Temperature Electrolyte Design for Lithium-Ion Batteries: Prospect and Challenges. *Chem. - Eur. J.* **2021**, *27*, 1−25.
(183) Liu, G.; Sun, Q.; Li, Q.; Zhang, J.; Ming, J. Electrolyte Issues in Lithium-Sulfur Batteries: Development, Prospect, and Challenges. *Energy Fuels* **2021**, *35*, 10405−10427.
(184) Zeng, Z.; Murugesan, V.; Han, K. S.; Jiang, X.; Cao, Y.; Xiao, L.; Ai, X.; Yang, H.; Zhang, J.-G.; Sushko, M. L.; Liu, J. Non-Flammable Electrolytes with High Salt-to-Solvent Ratios for Li-Ion and Li-Metal Batteries. *Nat. Energy* **2018**, *3*, 674−681.
(185) Wang, J.; Cui, Y. Electrolytes for Microsized Silicon. *Nat. Energy* **2020**, *5*, 361−362.
(186) Wen, B.; Deng, Z.; Tsai, P.-C.; Lebens-Higgins, Z. W.; Piper, L. F. J.; Ong, S. P.; Chiang, Y. M. Ultrafast ion Transport at a Cathode-Electrolyte Interface and its Strong Dependence on Salt Solvation. *Nat. Energy* **2020**, *5*, 578−586.
(187) Xue, W.; Huang, M.; Li, Y.; Zhu, Y. G.; Gao, R.; Xiao, X.; Zhang, W.; Li, S.; Xu, G.; Yu, Y.; Li, P.; Lopez, J.; Yu, D.; Dong, Y.; Fan, W.; Shi, Z.; Xiong, R.; Sun, C.-J.; Hwang, I.; Lee, W.-K.; Shao-Horn, Y.; Johnson, J. A.; Li, J. Ultra-High-Voltage Ni-rich Layered Cathodes in Practical Li Metal Batteries Enabled by a Sulfonamide-Based Electrolyte. *Nat. Energy* **2021**, *6*, 495−505.
(188) Chang, Z.; Qiao, Y.; Yang, H.; Deng, H.; Zhu, X.; He, P.; Zhou, H. Beyond the Concentrated Electrolyte: Further Depleting Solvent Molecules within a Li^+ Solvation Sheath to Stabilize High-Energy-Density Lithium Metal Batteries. *Energy Environ. Sci.* **2020**, *13*, 4122−4131.
(189) Wang, Z.; Sun, Z.; Shi, Y.; Qi, F.; Gao, X.; Yang, H.; Cheng, H. M.; Li, F. Ion-Dipole Chemistry Drives Rapid Evolution of Li Ions Solvation Sheath in Low-Temperature Li Batteries. *Adv. Energy Mater.* **2021**, *11*, 2100935.
(190) Qiu, H.; Du, X.; Zhao, J.; Wang, Y.; Ju, J.; Chen, Z.; Hu, Z.; Yan, D.; Zhou, X.; Cui, G. Zinc Anode-Compatible in-situ Solid Electrolyte Interphase via Cation Solvation Modulation. *Nat. Commun.* **2019**, *10*, 5374.
(191) Cao, L.; Li, D.; Hu, E.; Xu, J.; Deng, T.; Ma, L.; Wang, Y.; Yang, X.-Q.; Wang, C. Solvation Structure Design for Aqueous Zn Metal Batteries. *J. Am. Chem. Soc.* **2020**, *142*, 21404−21409.
(192) Zhang, Q.; Ma, Y.; Lu, Y.; Li, L.; Wan, F.; Zhang, K.; Chen, J. Modulating Electrolyte Structure for Ultralow Temperature Aqueous Zinc Batteries. *Nat. Commun.* **2020**, *11*, 4463.
(193) Liu, C.; Xie, X.; Lu, B.; Zhou, J.; Liang, S. Electrolyte Strategies toward Better Zinc-Ion Batteries. *ACS Energy Lett.* **2021**, *6*, 1015−1033.
(194) Zhang, Q.; Ma, Y.; Lu, Y.; Zhou, X.; Lin, L.; Li, L.; Yan, Z.; Zhao, Q.; Zhang, K.; Chen, J. Designing Anion-Type Water-Free Zn^{2+} Solvation Structure for Robust Zn Metal Anode. *Angew. Chem., Int. Ed.* **2021**, *60*, 23357−23364.
(195) Kopac Lautar, A.; Bitenc, J.; Rejec, T.; Dominko, R.; Filhol, J. S.; Doublet, M. L. Electrolyte Reactivity in the Double Layer in Mg Batteries: An Interface Potential-Dependent DFT Study. *J. Am. Chem. Soc.* **2020**, *142*, 5146−5153.
(196) Kartha, T. R.; Mallik, B. S. Structure and Transport of Solvent Ligated Octahedral Mg-Ion in an Aqueous Battery Electrolyte. *Chem. Eng. J.* **2021**, *66*, 1543−1554.
(197) Hou, S.; Ji, X.; Gaskell, K.; Wang, P.; Wang, L.; Xu, J.; Sun, R.; Borodin, O.; Wang, C. Solvation Sheath Reorganization Enables Divalent Metal Batteries with fast Interfacial Charge Transfer Kinetics. *Science* **2021**, *374*, 172−178.
(198) Sun, Y.; Zou, Q.; Wang, W.; Lu, Y.-C. Non-passivating Anion Adsorption Enables Reversible Magnesium Redox in Simple Non-nucleophilic Electrolytes. *ACS Energy Lett.* **2021**, *6*, 3607−3613.
(199) Yu, Z.; Juran, T. R.; Liu, X.; Han, K. S.; Wang, H.; Mueller, K. T.; Ma, L.; Xu, K.; Li, T.; Curtiss, L. A.; Cheng, L. Solvation Structure and Dynamics of $Mg(TFSI)_2$ Aqueous Electrolyte. *Energy Environ. Mater.* **2021**, DOI: 10.1002/eem2.12174.
(200) Jie, Y.; Tan, Y.; Li, L.; Han, Y.; Xu, S.; Zhao, Z.; Cao, R.; Ren, X.; Huang, F.; Lei, Z.; Tao, G.; Zhang, G.; Jiao, S. Electrolyte Solvation Manipulation Enables Unprecedented Room-Temperature Calcium-Metal Batteries. *Angew. Chem., Int. Ed.* **2020**, *59*, 12689−12693.
(201) Melemed, A. M.; Khurram, A.; Gallant, B. M. Current Understanding of Nonaqueous Electrolytes for Calcium-Based Batteries. *Batteries Supercaps* **2020**, *3*, 570−580.
(202) Pan, W.; Wang, Y.; Zhang, Y.; Kwok, H. Y. H.; Wu, M.; Zhao, X.; Leung, D. Y. C. A low-cost and Dendrite-Free Rechargeable Aluminium-Ion Battery with Superior Performance. *J. Mater. Chem. A* **2019**, *7*, 17420−17425.
(203) Yuan, D.; Zhao, J.; Manalastas, W.; Kumar, S.; Srinivasan, M. Emerging Rechargeable Aqueous Aluminum Ion Battery: Status, Challenges, and Outlooks. *Nano Mater. Sci.* **2020**, *2*, 248−263.
(204) Nian, Q.; Zhang, X.; Feng, Y.; Liu, S.; Sun, T.; Zheng, S.; Ren, X.; Tao, Z.; Zhang, D.; Chen, J. Designing Electrolyte Structure to Suppress Hydrogen Evolution Reaction in Aqueous Batteries. *ACS Energy Lett.* **2021**, *6*, 2174−2180.
(205) Ming, J.; Guo, J.; Xia, C.; Wang, W.; Alshareef, H. N. Zinc-Ion Batteries: Materials, Mechanisms, and Applications. *Mater. Sci. Eng. R Rep.* **2019**, *135*, 58−84.
(206) Zhao, J.; Yang, X.; Li, S.; Chen, N.; Wang, C.; Zeng, Y.; Du, F. Hybrid and Aqueous Li^+-Ni Metal Batteries. *CCS Chem.* **2021**, *3*, 2498−2508.